

# Proton-Transfer Polymerization by *N*-Heterocyclic Carbenes: Monomer and Catalyst Scopes and Mechanism for Converting Dimethacrylates into Unsaturated Polyesters

Miao Hong,<sup>†</sup> Xiaoyan Tang,<sup>†</sup> Laura Falivene,<sup>‡,§</sup> Lucia Caporaso,<sup>§</sup> Luigi Cavallo,<sup>\*,‡,§</sup> and Eugene Y.-X. Chen<sup>\*,†</sup>

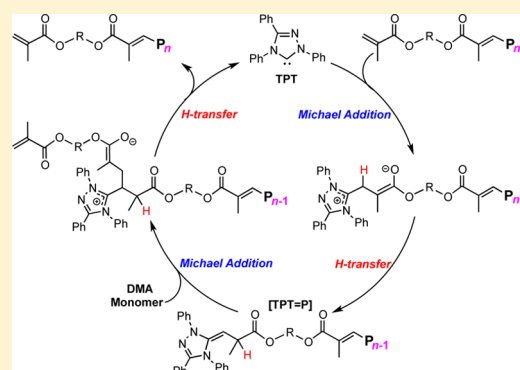
<sup>†</sup>Department of Chemistry, Colorado State University, Fort Collins, Colorado 80523-1872, United States

<sup>‡</sup>King Abdullah University of Science and Technology (KAUST), Physical Sciences and Engineering Division, Kaust Catalysis Center, Thuwal 23955-6900, Saudi Arabia

<sup>§</sup>Dipartimento di Chimica e Biologia, Università di Salerno, Via Papa Paolo Giovanni II, I-84084, Fisciano, Italy

## Supporting Information

**ABSTRACT:** This contribution presents a full account of experimental and theoretical/computational investigations into the *N*-heterocyclic carbene (NHC)-catalyzed proton-transfer polymerization (HTP) that converts common dimethacrylates (DMAs) containing no protic groups into unsaturated polyesters. This new HTP proceeds through the step-growth propagation cycles via enamine intermediates, consisting of the proposed conjugate addition–proton transfer–NHC release fundamental steps. This study examines the monomer and catalyst scopes as well as the fundamental steps involved in the overall HTP mechanism. DMAs having six different types of linkages connecting the two methacrylates have been polymerized into the corresponding unsaturated polyesters. The most intriguing unsaturated polyester of the series is that based on the biomass-derived furfuryl dimethacrylate, which showed a unique self-curing ability. Four MeO- and Cl-substituted TPT (1,3,4-triphenyl-4,5-dihydro-1*H*-1,2,4-triazol-5-ylidene) derivatives as methanol insertion products, <sup>Rx</sup>TPT(MeO/H) (R = MeO, Cl; x = 2, 3), and two free carbenes (catalysts), <sup>OMe2</sup>TPT and <sup>OMe3</sup>TPT, have been synthesized, while <sup>OMe2</sup>TPT(MeO/H) and <sup>OMe2</sup>TPT have also been structurally characterized. The structure/reactivity relationship study revealed that <sup>OMe2</sup>TPT, being both a strong nucleophile and a good leaving group, exhibits the highest HTP activity and also produced the polyester with the highest *M<sub>n</sub>*, while the Cl-substituted TPT derivatives are least active and efficient. Computational studies have provided mechanistic insights into the tail-to-tail dimerization coupling step as a suitable model for the propagation cycle of the HTP. The extensive energy profile was mapped out, and the experimentally observed unicity of the TPT-based catalysts was satisfactorily explained with the thermodynamic formation of key spirocyclic species.



## INTRODUCTION

The sustained rise of organopolymerization,<sup>1</sup> which uses small-molecule organic compounds as catalysts or initiators in polymer synthesis and becomes a preferred method especially when metal-free products or processes are of primary concern, has profited from the emergence of powerful organic catalysts and unique mechanistic pathways developed in the rapidly growing field of organocatalysis.<sup>2</sup> A prominent class of organic catalysts that attracted increasing attention is *N*-heterocyclic carbenes (NHCs), due to their inherently high Brønsted basicity and nucleophilicity that brought about unique reactivity and selectivity often observed in many different types of organic reactions.<sup>3</sup> Thanks to the pioneering work of Hedrick, Waymouth, and their co-workers,<sup>4</sup> the utility of the NHC-mediated reactions has been expanded to polymer synthesis through NHC-mediated polymerizations,<sup>5</sup> via predominantly the ring-opening polymerization (ROP) of heterocyclic

monomers, such as lactides,<sup>6</sup> lactones,<sup>7</sup> epoxides,<sup>8</sup> cyclic carbonates,<sup>9</sup> cyclic (carbo)siloxanes,<sup>10</sup> and *N*-carboxyl-anhydrides.<sup>11</sup> NHC-mediated step-growth polymerization has been reported as well.<sup>12</sup> Polymerization of acrylic monomers such as methyl methacrylate (MMA) has also been realized through the group-transfer polymerization initiated by a silyl ketene acetal (SKA),<sup>13</sup> using NHCs as alternative nucleophilic catalysts for activating the SKA initiator.<sup>14</sup> Such acrylic monomers can be rapidly polymerized by frustrated Lewis pairs (FLPs)<sup>15</sup> consisting of bulky NHC bases, such as the Arduengo carbenes 1,3-di-*tert*-butylimidazolin-2-ylidene (*t*Bu), and 1,3-dimesitylimidazolin-2-ylidene (IMes),<sup>16</sup> and the strongly acidic, sterically encumbered alane Al(C<sub>6</sub>F<sub>5</sub>)<sub>3</sub>, via the proposed zwitterionic imidazolium enolaluminate intermediates.<sup>17</sup>

Received: December 13, 2015

Published: January 18, 2016

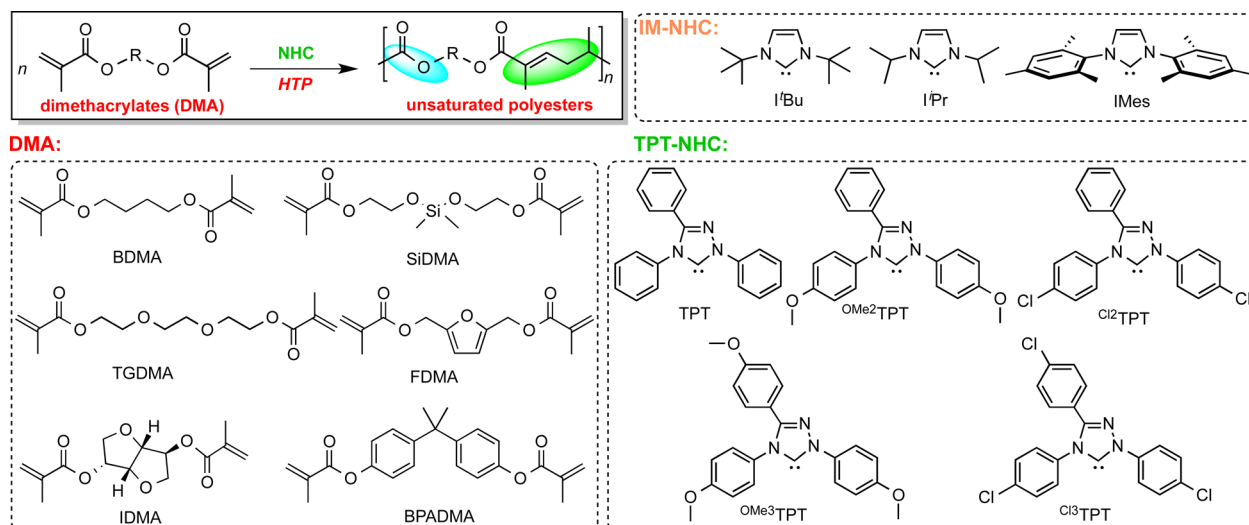


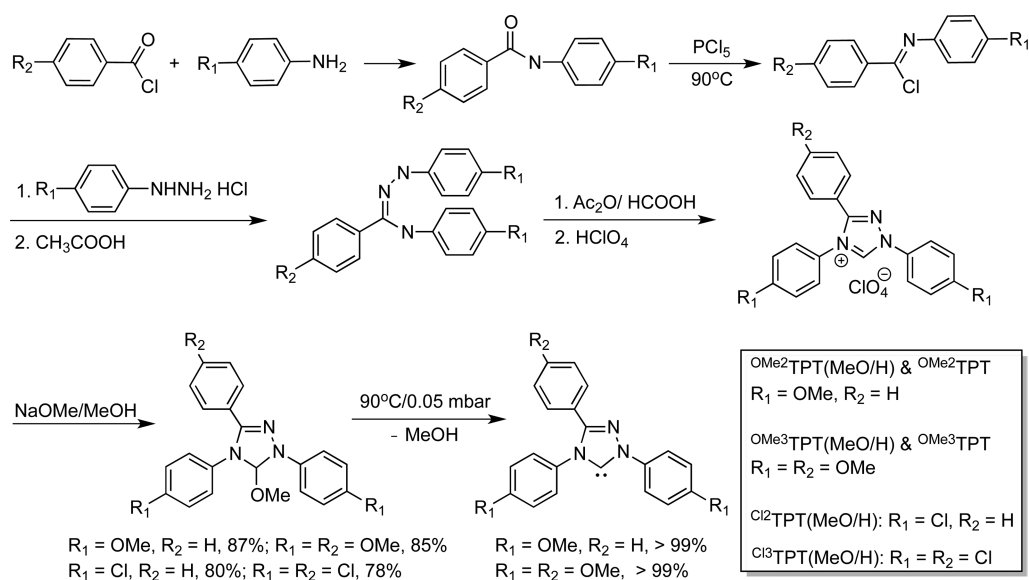
**Figure 1.** Structures of dimethacrylate (DMA) monomers, NHC catalysts, and unsaturated polyesters investigated in this study.

For  $\alpha,\beta$ -unsaturated esters or acrylic monomers, an important class of Michael acceptors, there exhibits an exquisite selectivity of the substrate or monomer structure to the NHC structure, as shown by the following *five* types of reactions observed between such substrates and NHCs. Fu et al.<sup>18</sup> reported the first intramolecular umpolung of  $\alpha,\beta$ -unsaturated esters carrying a  $\omega$ -pendant leaving group to form  $\beta$ -alkylation/cyclization products, using triazolylidene carbenes such as the Enders TPT (1,3,4-triphenyl-4,5-dihydro-1H-1,2,4-triazol-5-ylidene).<sup>19</sup> With common methacrylates such as MMA, we found that the imidazolylidene carbene IMes, which was estimated to be  $10^3$  times more nucleophilic than TPT,<sup>21</sup> reacts with the substrate to form a stable *single-addition* product, an enamine; the formation of the enamine, or the deoxy-Breslow intermediate,<sup>22</sup> analogous to the Breslow intermediate<sup>23</sup> involved in the benzoin condensation reaction,<sup>24</sup> was proposed to proceed through the initial Michael (conjugate) addition of IMes to MMA to form the corresponding zwitterionic enolate intermediate followed by proton transfer. Glorius<sup>25</sup> and Matsuoka<sup>26</sup> discovered that TPT catalyzes tail-to-tail umpolung *dimerization* of MMA and other methacrylates, carried out typically at 80 °C, while the common imidazolylidene carbenes such as IMes are ineffective. Subsequently, analogous dimerization of methacrylonitrile,<sup>27</sup> styrenes,<sup>28</sup> other vinyl compounds (including 2-vinylpyridine, acrylonitrile, dimethyl acrylamide, and various functionalized acrylates),<sup>29</sup> and crotonates (by I'PrMe<sub>2</sub>, 1,3-di-isopropyl-4,5-dimethylimidazol-2-ylidene)<sup>30</sup> has also been recently realized. Switching the NHC to I'Pr (1,3-di-isopropylimidazol-2-ylidene), Taton et al. recently found this NHC promotes *cyclodimerization* of MMA to form an imidazolium-enolate cyclodimer.<sup>31</sup> On the other hand, Matsuoka et al. revealed that IMes catalyzes *cyclotetramerization* of acrylates.<sup>32</sup> Intriguingly, I'Bu promotes *polymerization* of MMA in dimethylformamide (DMF) at room temperature (RT) to produce PMMA with  $M_n$  (number-average molecular weight) = 33.2 kg/mol and  $D$  ( $M_w/M_n$ ) = 1.99.<sup>20</sup> We also revealed that I'Bu catalyzes rapid polymerization of  $\gamma$ -methyl- $\alpha$ -methylene- $\gamma$ -butyrolactone, a biorenewable cyclic analogue of MMA, converting quantitatively 3000 or 10000 equiv of the monomer in 1 or 5 min at RT to the corresponding bioplastics.<sup>33</sup> Buchmeiser et al. showed that MMA can also be polymerized by the CO<sub>2</sub>-protected NHC

latent precatalyst, I'Bu-CO<sub>2</sub>.<sup>34</sup> Taton et al. recently reported the polymerization of MMA by I'Bu in the presence of alcohol to produce PMMA and  $\alpha$ -alkoxy PMMA ( $M_n$  up to 8000 g/mol), via both Michael and oxa-Michael addition pathways.<sup>35</sup>

Proton-transfer polymerization (HTP) describes a polymerization in which each propagation step involves a proton transfer,<sup>36</sup> a process to (re)generate the active propagating species or activate the monomer or the nucleophile. For acrylic monomers, in the 1950s scientists at Hercules showed that the anionic polymerization of acrylamide (CH<sub>2</sub>=CHCONH<sub>2</sub>) afforded poly( $\beta$ -alanine), instead of the anticipated polyacrylamide,<sup>37</sup> which was proposed to proceed through the intermolecular hydrogen transfer, first to monomer, then to dimer, trimer, etc.<sup>38</sup> Subsequently, base-catalyzed HTP processes of acrylic acid to poly( $\beta$ -propiolactone),<sup>39</sup> hydroxyalkyl acrylates to poly(ester-ether)s,<sup>40</sup> acrylates containing two hydroxyl groups to hyperbranched poly(ester-ether)s,<sup>41</sup> 2-hydroxyethyl (meth)acrylates to oligo(ether-ester)s,<sup>42</sup> 2-hydroxyethyl methacrylate to a hyperbranched polymethacrylate,<sup>43</sup> and *N,N*-bis(2-hydroxyalkyl (meth)acrylamides to hyperbranched poly(ether-amide)s<sup>44</sup> have been reported. Most recently, Matsuoka et al. reported the polymerization of hydroxyalkyl acrylates by an NHC catalyst (TPT), producing low MW poly(ester-ether)s with  $M_n$  up to 2400 g/mol ( $D$  = 3.8).<sup>45</sup> This NHC-mediated polymerization was proposed to proceed via an initial zwitterionic intermediate, derived from Michael addition of TPT to the monomer, followed by a proton transfer from the HO-carrying moiety to generate the alkoxide which undergoes oxa-Michael addition to the monomer, followed by another proton transfer to complete a propagation cycle.<sup>45</sup> For epoxide monomers, Fréchet et al. developed a base-catalyzed HTP of H-AB<sub>2</sub> type monomers to produce hyperbranched epoxy or hydroxyl functionalized polymers (aromatic epoxides) through repeated nucleophilic ring-opening and proton-transfer processes, the latter of which is to activate the monomer to generate the stronger nucleophile (A<sup>o</sup>-B<sub>2</sub>) for the epoxide ring-opening.<sup>36,46</sup> This strategy has also been employed for the synthesis of hyperbranched polyesters<sup>47</sup> and porphyrins.<sup>48</sup> More recently, Khan et al. reported the HTP of H-AB<sub>2</sub> monomer bearing two epoxide and a thiol groups to produce a polythioether-based hyperbranched polymer.<sup>49</sup>

Scheme 1. Outlined Synthetic Route to MeO- and Cl-Substituted TPT Derivatives as Methanol Insertion Products and Also as Free Carbenes



It can be seen from the above overview, the monomers applicable to HTP are acrylic and epoxide monomers bearing acidic protons, typically OH group(s).<sup>50</sup> Departing from this conventional HTP process, we<sup>51</sup> recently disclosed a new type of HTP by an NHC catalyst that enables polymerization of common acyclic monomers containing no such protic groups, like typical dimethacrylates, uniquely into *unsaturated polyesters*, instead of forming typical poly(methacrylate)s via vinyl-addition pathways by any other polymerization methods (Figure 1). Such unsaturated polyesters, which are of scientific and technological interest for producing tailor-made polyester materials through postfunctionalization and cross-linking,<sup>52</sup> exhibit high thermal stability and can be subsequently cross-linked to robust polyester materials.<sup>51</sup> This unconventional HTP is catalyzed by a selective NHC [TPT or methoxytriazoline, TPT(MeO/H)] capable of promoting intermolecular umpolung condensation coupling via *proton transfer* and proceeds through the step-growth propagation cycles via enamine intermediates, consisting of the proposed Michael (conjugate) addition–proton transfer–NHC release fundamental steps.<sup>51</sup> It is revealed that the added suitable phenol plays a critical role in achieving an effective HTP: shutting down the radically induced chain-growth addition polymerization under HTP conditions (typically at 80–120 °C) and facilitating proton transfer following each monomer enchainment. As typical acrylic monomers are currently converted exclusively through polyadditions across C=C double bonds into nonbiodegradable polyacrylates on large industrial scales, this HTP step-growth process offers new polymer products from readily available acrylic monomers in the form of degradable polyesters, is a metal-free process, splits off no small molecules, and therefore is 100% atom-economical, thus bearing hallmarks of the green chemistry. However, two important fundamental aspects of this new HTP are largely unaddressed or currently unknown: mechanistic details as well as monomer and catalyst scopes. Accordingly, the central objective of this study was to address these questions through combined experimental and theoretical/computational investigations, the results of which are presented herein.

## RESULTS AND DISCUSSION

**Synthesis and Characterization of New TPT Derivatives.** As imidazolydene (IM) carbenes such as *t*Bu and IMes are ineffective in promoting the HTP of DMAs while the triazolylidene carbene TPT is highly effective for this HTP,<sup>51</sup> we used TPT as a guide in our computational screening to identify other potentially effective NHC catalysts. In this context, we found MeO- and Cl-substituted TPT derivatives are promising, whose energetics is similar to TPT (*vide infra*). Accordingly, we set out to synthesize such TPT derivatives.

Scheme 1 outlines the procedures used for the synthesis of four MeO- and Cl-substituted TPT derivatives as precatalysts (methanol insertion products), OMe<sub>2</sub>TPT(MeO/H), OMe<sub>3</sub>TPT(MeO/H), Cl<sub>2</sub>TPT(MeO/H), and Cl<sub>3</sub>TPT(MeO/H), as well as catalysts in the form of free carbenes, OMe<sub>2</sub>TPT and OMe<sub>3</sub>TPT, starting from commercially available MeO- and Cl-substituted acyl chloride and aniline. Deprotonation of the MeO-substituted triazolium salts [OMe<sub>3</sub>TPT]ClO<sub>4</sub> and [OMe<sub>2</sub>TPT]ClO<sub>4</sub><sup>18</sup> with NaOMe/MeOH readily afforded the pure methoxytriazolines OMe<sub>2</sub>TPT(MeO/H) and OMe<sub>3</sub>TPT(MeO/H) in good yields (85–87%).<sup>53</sup> The characteristic resonances for the NCHOCH<sub>3</sub> and NCHOCH<sub>3</sub> protons appear at  $\delta$  6.65 and 3.13 ppm for OMe<sub>2</sub>TPT(MeO/H) and  $\delta$  6.68 and 3.18 ppm for OMe<sub>3</sub>TPT(MeO/H). Major ion peaks at *m/z* 358.10 and 388.16 were observed in high-resolution mass spectroscopy (HRMS) spectra of OMe<sub>2</sub>TPT(MeO/H) and OMe<sub>3</sub>TPT(MeO/H), respectively, which are 31 mass units lower than the theoretical values [389.17 for OMe<sub>2</sub>TPT(MeO/H) and 420.47 for OMe<sub>3</sub>TPT(MeO/H)], due to the loss of the methoxyl group during the analysis. Single crystals of OMe<sub>2</sub>TPT(MeO/H) suitable for X-ray crystallographic studies were grown from MeOH at –20 °C and its molecular structure was confirmed by X-ray diffraction analysis (Figure 2). The metric parameters are comparable with those of the parent TPT(MeO/H).<sup>19</sup>

Free carbenes OMe<sub>2</sub>TPT and OMe<sub>3</sub>TPT were obtained in quantitative yields via thermal  $\alpha$ -elimination of methanol from their corresponding methoxytriazolines at 90 °C/0.05 mbar. Compared with OMe<sub>3</sub>TPT(MeO/H), which required 32 h of thermal treatment to completely remove the methanol to yield

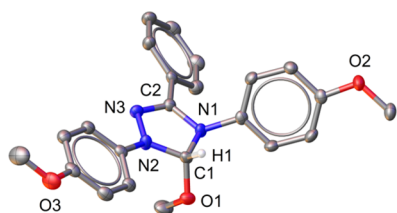


**Figure 2.** X-ray crystal structure of  $^{\text{OMe}2}\text{TPT}(\text{MeO}/\text{H})$ . Hydrogen atoms (except H1) omitted for clarity and ellipsoids drawn at 50% probability. Selected bond lengths (Å) and angles (deg): C(1)–N(1), 1.458(6); C(1)–H(1), 1.000(4); C(1)–O(1), 1.413(5); C(1)–N(2), 1.451(6); H(1)–C(1)–N(1), 109.8(4); H(1)–C(1)–N(2), 109.8(4); H(1)–C(1)–O(1), 109.8(4); N(1)–C(1)–N(2), 100.2(3); H(1)–C(1)–O(1), 113.5(4).

the pure free carbene, the methanol elimination from  $^{\text{OMe}2}\text{TPT}(\text{MeO}/\text{H})$  was faster, producing the pure free  $^{\text{OMe}2}\text{TPT}$  in 24 h. This elimination process can be readily monitored by  $^1\text{H}$  NMR, which showed gradually disappearance of the  $\text{NCHOCH}_3$  protons in the methanol adduct upon formation of the free carbene (Figure 3).  $^{13}\text{C}$  NMR further confirmed the successful formation of the free carbenes, as evidenced by the characteristic chemical shifts corresponding to the carbene carbon<sup>19</sup> at  $\delta$  213.2 and 212.6 ppm for  $^{\text{OMe}2}\text{TPT}$  and  $^{\text{OMe}3}\text{TPT}$ , respectively. Lastly, the molecular structure of the free carbene  $^{\text{OMe}2}\text{TPT}$  was confirmed by single-crystal X-diffraction analysis (Figure 4). Compared with  $^{\text{OMe}2}\text{TPT}(\text{MeO}/\text{H})$ , the most significant change in metric parameters are the shorten the C(1)–N bonds by  $\sim 0.1$  Å upon formation of the carbene, from 1.458(6) and 1.451(6) Å in  $^{\text{OMe}2}\text{TPT}(\text{MeO}/\text{H})$  to 1.349(2) and 1.376(2) Å in  $^{\text{OMe}2}\text{TPT}$ , while the N–C(1)–N angle remained essentially the same ( $100.2^\circ$ ), which is typical of a singlet carbene.

Procedures for the preparation of MeO-substituted [TPT]- $\text{ClO}_4$  and  $\text{TPT}(\text{MeO}/\text{H})$  were modified to synthesize Cl-substituted derivatives. It is imperative that, in the deprotonation step of converting the Cl-substituted triazolium salts [ $^{\text{Cl}3}\text{TPT}$ ] $\text{ClO}_4$  and [ $^{\text{Cl}2}\text{TPT}$ ] $\text{ClO}_4$  with  $\text{NaOMe}/\text{MeOH}$ , the reaction be carried out in a short time ( $<15$  min) as prolonged reaction times induced decomposition to form side products, as shown by monitoring the reaction with  $^1\text{H}$  NMR. After purification by recrystallization,  $^{\text{Cl}2}\text{TPT}(\text{MeO}/\text{H})$  and  $^{\text{Cl}3}\text{TPT}(\text{MeO}/\text{H})$  were obtained in good yields (78–80%). The

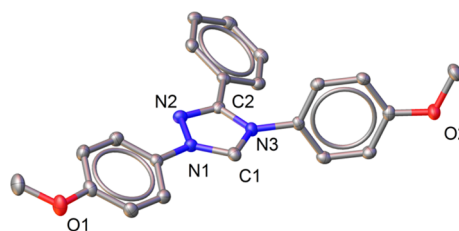


**Figure 4.** X-ray crystal structure of the free carbene  $^{\text{OMe}2}\text{TPT}$ . Hydrogen atoms omitted for clarity and ellipsoids drawn at 50% probability. Selected bond lengths (Å) and angles (deg): C(1)–N(1), 1.349(2); C(1)–N(3), 1.376(2); N(1)–C(1)–N(3), 100.16(3).

characteristic resonances for the  $\text{NCHOCH}_3$  and  $\text{NCHOCH}_3$  protons appear at  $\delta$  6.29 and 2.88 ppm for  $^{\text{Cl}2}\text{TPT}(\text{MeO}/\text{H})$  and 6.24 and 2.84 ppm for  $^{\text{Cl}3}\text{TPT}(\text{MeO}/\text{H})$ . However, different from the MeO-substituted TPT derivatives, generation of the free carbene from  $^{\text{Cl}2}\text{TPT}(\text{MeO}/\text{H})$  or  $^{\text{Cl}3}\text{TPT}(\text{MeO}/\text{H})$  was unsuccessful via  $\alpha$ -elimination of methanol; upon heating at  $90^\circ\text{C}/0.05$  mbar for up to 36 h, the NMR signals due to the precursors gradually reduced, but the resulting (unidentifiable) species gave a messy NMR spectrum and had no polymerization activity when tested for the HTP of DMAs. These results indicated that the methanol elimination from the Cl-substituted TPT derivatives is a slow process and, more importantly, the resulting free carbene is not thermally stable (in the absence of monomer) under such conditions. Hence, the precatalysts  $^{\text{Cl}2}\text{TPT}(\text{MeO}/\text{H})$  and  $^{\text{Cl}3}\text{TPT}(\text{MeO}/\text{H})$  were used directly for the HTP polymerization studies carried out in the presence of monomer at relatively high temperature of  $110^\circ\text{C}$  so that the catalyst, once generated *in situ*, is immediately reacted with the monomer.

#### Fundamental Reactions of Dimethacrylates with TPT.

HTP promoted by  $\text{TPT}^{\text{S}1}$  was proposed to proceed through the step-growth propagation cycles via enamine intermediates [ $\text{TPT}=\text{P}$ ], consisting of repeated Michael (conjugate) addition–proton transfer–NHC (TPT) release fundamental steps (Scheme 2). In this work, DMAs with six different types of linkages connecting the two methacrylate moieties were utilized for the HTP studies, including 1,4-butanediol dimethacrylate (BDMA) with an *alkyl* linker, triethylene glycol dimethacrylate (TGDMA) with an *ether* linker, 2,2'-[(dimethylsilylene)dioxy] dimethacrylate (SiDMA) with a *silyl*

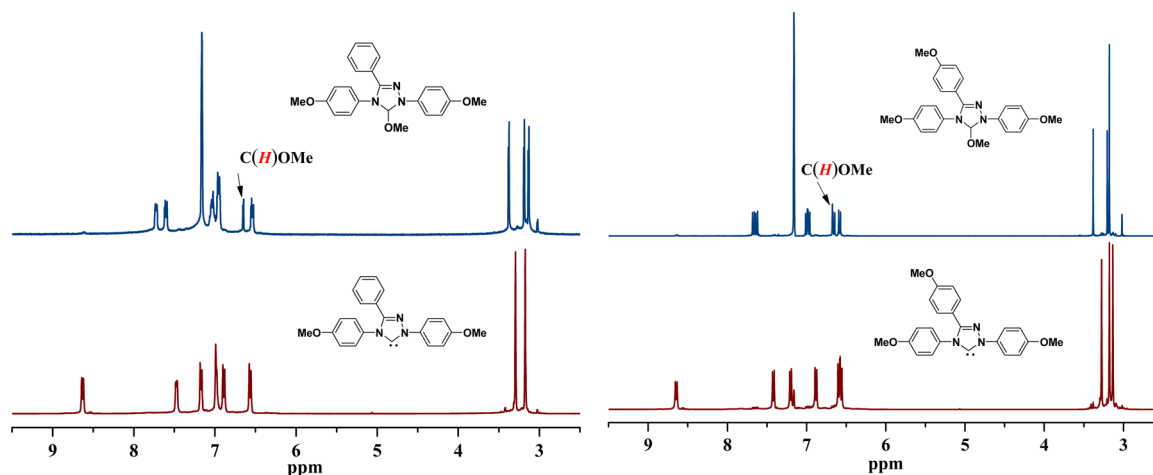


**Figure 3.** Comparisons of  $^1\text{H}$  NMR ( $\text{C}_6\text{D}_6$ ) spectra of the methanol insertion products (top) and the free carbenes (bottom).

## Scheme 2. Proposed Propagation Cycle for the HTP of DMA by TPT to Unsaturated Polyesters

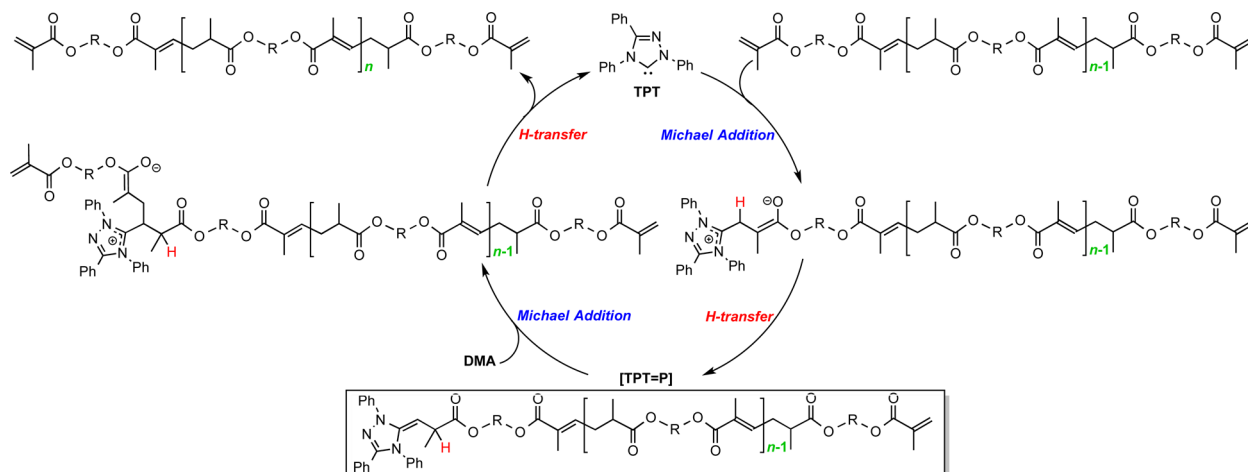


**Table 1. Conversion Data of DMAs in the Formation of Bis(enamine) Intermediates and Polyesters by TPT Performed in J. Young-type NMR Tubes<sup>a</sup>**

Run	DMA	DMA/TPT/MP	Temp. (°C)	Conv. (%) <sup>b</sup>			
				10 min	60 min	3 h	Longer time
1	BDMA	1/2/0	25	7.20	40.2	63.0	83.8 (24 h)
2	SiDMA	1/2/0	25	23.4	72.7	86.1	96.2 (10 h)
3	TGDMA	1/2/0	25	37.7	76.9	87.6	100 (7 h)
4	FDMA	1/2/0	25	57.3	83.8	90.0	100 (6 h)
5	IDMA	1/2/0	25	68.4	91.0	100.0	
6	BPADMA	1/2/0	25	76.8	100 <sup>c</sup>		
7	BDMA	5/1/0.1	80		72.0	98.4	100 (6 h)
8	SiDMA	5/1/0.1	80		54.3	83.8	96.4 (7 h)
9	TGDMA	5/1/0.1	80		86.6	100	
10	FDMA	5/1/0.1	80		69.0	100	
11	IDMA	5/1/0.1	80		100		
12	BPADMA	5/1/0.1	80		86.0 <sup>c</sup>	100 <sup>c</sup>	

<sup>a</sup>Conditions: TPT = 14.9 mg (0.05 mmol), DMA = 0.025 mmol in 0.50 mL toluene-*d*<sub>8</sub> for runs 1–6, DMA = 0.25 mmol in 0.25 mL toluene-*d*<sub>8</sub> for runs 7–12, MP (4-methoxyphenol) = 0.62 mg (0.005 mmol) in 0.25 mL toluene-*d*<sub>8</sub>. <sup>b</sup>Conv.(%) = monomer conversion measured by <sup>1</sup>H NMR spectroscopy. <sup>c</sup>BPADMA monomer consumed but accompanied by some side reactions.

ether linker, 2,5-bis(hydroxymethyl)furan dimethacrylate (FDMA) with a furan linker, isosorbide dimethacrylate (IDMA) with a bicyclic linker, and bisphenol A dimethacrylate (BPADMA) with an aromatic linker. Among these dimethacrylates, BDMA, TGDMA and BPADMA are commercially available, SiDMA was prepared by the reaction of chlorodimethylsilane and 2-hydroxyethyl methacrylate, while FDMA and IDMA are biomass-derived and were prepared by the reaction of the corresponding diol and methacryloyl chloride.<sup>53</sup>

To ascertain the influence of monomer structure on the HTP activity, the formation of bis(enamine) intermediates and the resulting polyesters was investigated through monitoring stoichiometric and polymerization reactions by <sup>1</sup>H NMR. First, the formation of bis(enamine) intermediates was studied by treating 2 equiv of TPT with 1 equiv of DMA in toluene-*d*<sub>8</sub> at RT [note that the 1:1 reaction produced a mixture of mono- and bis(enamine) adducts]. The conversion data of different DMAs are summarized in Table 1 and <sup>1</sup>H NMR spectra of the reaction of FDMA + 2 TPT toward the formation of the bis(enamine) intermediate FDMA(TPT)<sub>2</sub> at different times are provided in Figure 5, while the <sup>1</sup>H NMR spectra for the reaction with other DMAs are included in Figures S5–8 of the SI. The reactivity was found to increase in the following the

order: BDMA < SiDMA < TGDMA < FDMA < IDMA < BPADMA, which apparently correlates with increasing the electron deficiency of the methacrylate double bond and the rigidity of the DMA structure. Among these monomers, IDMA exhibited the second highest reactivity, which achieved 68.4% conversion in 10 min (run 5, Table 1), while BDMA displays the lowest reactivity, which reached a lower conversion of 63.0% even after 3 h (run 1, Table 1). BPADMA, although its enamine formation with TPT was the fastest, achieving 76.8% monomer conversion in 10 min, afforded some light yellow solid which gradually precipitated from the solution after longer reaction time (1 h), due to unknown side reactions (run 6, Table 1). As a result, the peaks of the bis(enamine) intermediate in the <sup>1</sup>H NMR spectrum (Figure S8) obtained at a late stage of reaction became broad with some amount of TPT remained unreacted while BPADMA consumed completely at the end of reaction.

Next, the HTP in a DMA/TPT/MP ratio of 5/1/0.1 performed in J. Young-type NMR tubes at 80 °C was followed by <sup>1</sup>H NMR, where a small amount of MP (4-methoxyphenol) was added to inhibit thermally (radically) induced vinyl addition side polymerization.<sup>51</sup> As can be seen from runs 7–12 (Table 1), all DMA monomers can be readily polymerized,

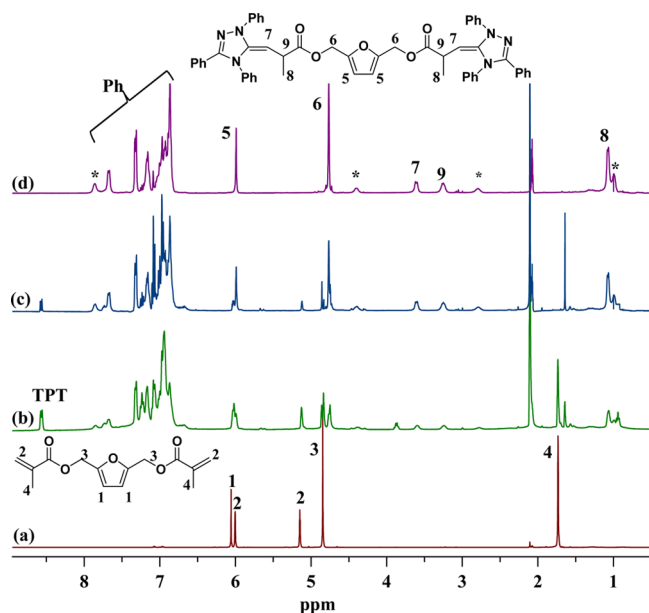


**Figure 5.**  $^1\text{H}$  NMR (toluene- $d_8$ , 25  $^\circ\text{C}$ ) spectra of the reaction of FDMA + 2 TPT toward formation of the bis(enamine) intermediate FDMA(TPT) $_2$  at different times: (a) FDMA monomer; (b) after 10 min (57.3% conversion); (c) after 60 min (90.0% conversion); (d) after 6 h (100% conversion). Peaks marked as \* are characteristic of the minor isomer of the bis(enamine) intermediate.

with increasing the polymerization activity in the order of: SiDMA < BDMA  $\approx$  FDMA < TGDMA  $\approx$  BPADMA < IDMA, which is somewhat different from the reactivity trend observed for the bis(enamine) intermediate formation (BDMA < SiDMA < TGDMA < FDMA < IDMA < BPADMA). For FDMA (Figure 6) and TGDMA, a quantitative conversion was

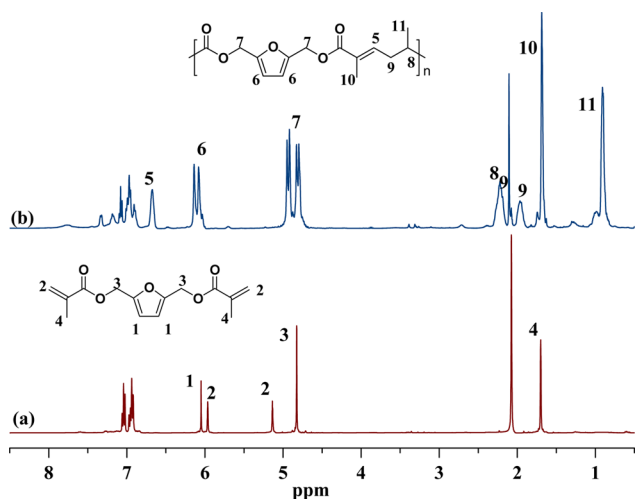


**Figure 6.**  $^1\text{H}$  NMR spectra (toluene- $d_8$ ) of the HTP of FDMA (FDMA/TPT/MP = 5/1/0.1) in a J-Young NMR tube: (a) 10 min, 25  $^\circ\text{C}$ , 10 min; (b) 80  $^\circ\text{C}$ , 3 h (100% conversion).

achieved in 3 h (runs 9 and 10), but for IDMA a quantitative conversion was achieved in 1 h (run 11). As in the case of bis(enamine) intermediate formation, some side reactions were accompanied in the HTP of BPADMA upon achieving quantitative monomer conversion (Figure S12).

**Polymerization of Dimethacrylates with TPT.** Table 2 summarizes the polymerization results obtained from the

preparative scale polymerization runs. As these polymerizations are only effective when carried out at temperature  $\geq 80$   $^\circ\text{C}$ , a small amount of the radical inhibitor such as MP is added, which not only effectively shuts down the radically induced vinyl-addition chain-growth pathway but also enhances the activity of the step-growth polymerization by facilitating the proton-transfer process.<sup>51</sup> Hence, in the presence of 0.1 mol % (or 0.02 equiv. relative to TPT) of MP, the polymerization of BDMA by TPT (5 mol %) in toluene at 80  $^\circ\text{C}$  led to *exclusive* formation of the unsaturated polyester PBDMA with  $M_n = 9.42$  kg/mol and  $\mathcal{D} = 1.90$  (run 1, Table 2), without formation of any detectable amount of the vinyl-addition polymer. The polymerization with a lower TPT loading of 1 mol % in a BDMA/TPT/MP ratio of 100/1/0.1 produced PBDMA with a significantly higher  $M_n$  of 14.2 kg/mol and  $\mathcal{D} = 1.70$  (run 2, Table 2) at 100  $^\circ\text{C}$ , or with  $M_n = 15.8$  kg/mol and  $\mathcal{D} = 1.73$  at 110  $^\circ\text{C}$  (run 3, Table 2). However, the polymerization performed at a further higher temperature of 120  $^\circ\text{C}$  became uncontrolled and gelled in 3 h, producing PBDMA with a low molecular weight, plus the vinyl-addition polymer.<sup>51</sup>

Consistent with the relative activity observed in the polymerizations performed in J-Young NMR tubes with a high catalyst loading of 20 mol % (*vide supra*), SiDMA exhibited the lowest activity (run 4, Table 2) compared with other monomers. For TGDMA, the polymerization at 80  $^\circ\text{C}$  with a 5 mol % TPT loading reached quantitative monomer conversion in 12 h, producing PTGDMA with a relatively high  $M_n$  of 15.3 kg/mol (run 5, Table 2). Decreasing the catalyst loading to 1 mol % and increasing the polymerization temperature to 100  $^\circ\text{C}$  achieved quantitative conversion in 24 h, and the resulting polymer still had relatively high molecular weight (run 6 vs 5, Table 2). In the case of the biomass-derived FDMA, the use of 2 mol % of MP (relative to TPT) can not prevent thermally induced radical polymerization any more, and the resulting polyester contained some vinyl addition polymer (confirmed by  $^1\text{H}$  NMR) which brought about a broad molecular weight distribution ( $\mathcal{D} = 3.02$ , run 7, Table 2). However, this problem can be easily overcome by employing 10 mol % MP, which yielded the pure polyester with  $M_n = 10.7$  kg/mol and  $\mathcal{D} = 2.63$  (run 8, Table 2). Decreasing the catalyst loading to 1 mol % and increasing the polymerization temperature to 100  $^\circ\text{C}$  did not further increase the polymer molecular weight (run 9 vs 8, Table 2). For the other biomass-derived monomer with a more rigid structure, the polymerization of IDMA became less controlled. Even in the presence of 10 mol % of MP, the polymerization still gelled in 2 h with formation of the vinyl-addition polymer side product, with the resulting polymer exhibiting a bimodal molecular weight distribution (run 10, Table 2). To prevent the vinyl addition polymerization, the amount of MP was increased to 20 mol %, under which conditions the polymerization went smoothly and achieved quantitative monomer conversion in 12 h, affording the pure polyester with  $M_n = 10.9$  kg/mol and  $\mathcal{D} = 2.30$  (run 11, Table 2). Finally, in the case of BPADMA polymerization, due to side reactions (*vide supra*), the isolated polymer yield was only 56%, although the monomer was consumed completely in 24 h (run 12, Table 2).

The structure of the resulting unsaturated polyesters with the unique umpolung linkage  $-\text{[C(Me)=CH-CH}_2\text{-CH(Me)]}_n-$ ,<sup>51</sup> can be readily identified by resonances appeared at  $\delta$  6.7 ( $E/Z = 96/4$ ), 2.2–2.7, 1.8, and 1.2 ppm in  $^1\text{H}$  NMR spectra (Figures 7 and 8). All resonances in the  $^1\text{H}$  NMR spectra were readily assigned, except for the bicyclic ring

Table 2. Results of HTP of Dimethacrylates by TPT<sup>a</sup>

Run	DMA	DMA/TPT/MP	Temp. (°C)	Time (h)	Conv. <sup>b</sup> (%)	M <sub>n</sub> <sup>c</sup> (kg/mol)	D <sup>c</sup> (M <sub>w</sub> /M <sub>n</sub> )
1	BDMA	20/1/0.02	80	24	100	9.42	1.90
2	BDMA	100/1/0.1	100	48	100	14.2	1.70
3	BDMA	100/1/0.1	110	24	100	15.8	1.73
4	SiDMA	20/1/0.02	80	24	89.0	4.42	1.35
5	TGDMA	20/1/0.02	80	12	100	15.3	2.02
6	TGDMA	100/1/0.1	100	24	100	11.2	1.68
7	FDMA	20/1/0.02	80	12	100	14.4	3.02
8	FDMA	20/1/0.10	80	6	100	10.7	2.63
9	FDMA	100/1/0.2	100	24	100	9.52	2.27
10	IDMA	20/1/0.10	80	2	78.0	5.29(176)	1.81(1.36)
11	IDMA	20/1/0.20	80	12	100	10.9	2.30
12	BPADMA	20/1/0.10	80	24	100 <sup>d</sup>	4.11	1.40

<sup>a</sup>Conditions: [monomer] = 1.6 M in toluene. <sup>b</sup>Conv.(%) = monomer conversion measured by <sup>1</sup>H NMR spectroscopy. <sup>c</sup>Number-average molecular weight (M<sub>n</sub>) and molecular weight distribution (D = M<sub>w</sub>/M<sub>n</sub>) determined by GPC at 40 °C in DMF relative to PMMA standards. <sup>d</sup>Isolated yield was only 56%, due to side reactions.

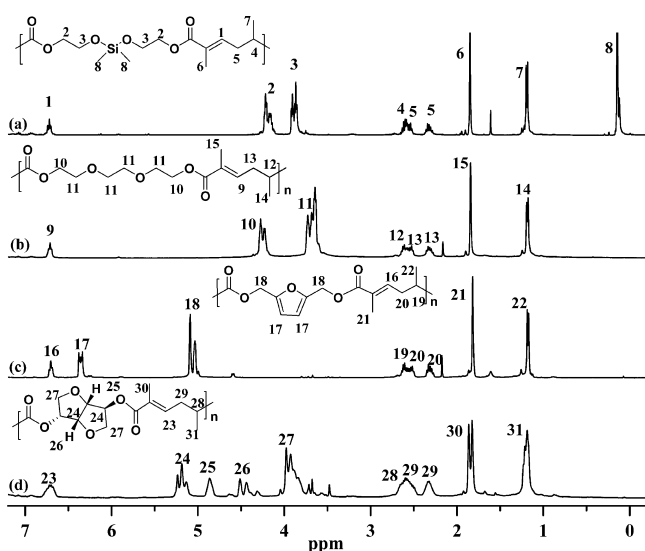


Figure 7. <sup>1</sup>H NMR (CDCl<sub>3</sub>) spectra of selected unsaturated polyesters: (a) PSiDMA (run 4, Table 2), (b) PTGDMA (run 5, Table 2), (c) PFDMA (run 8, Table 2), (d) PIDMA (run 11, Table 2).

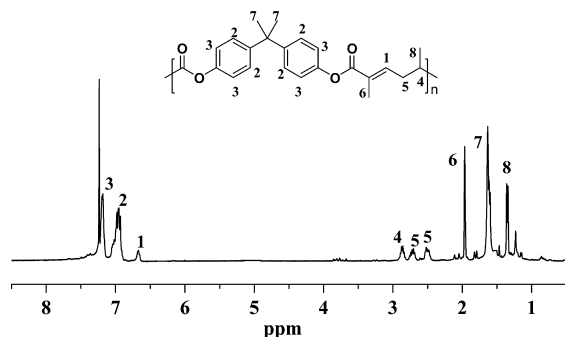


Figure 8. <sup>1</sup>H NMR (CDCl<sub>3</sub>) spectrum of PBPADMA (run 12, Table 2).

protons in the case of PIDMA. Nevertheless, these protons on the cyclic ring were assigned with the assistance of <sup>1</sup>H–<sup>1</sup>H COSY, the correct connectivity of which was clearly shown by correlation of the peaks marked in Figure S17. The structures of the obtained unsaturated polyesters were further confirmed by <sup>13</sup>C NMR spectra (Figures S15–16). The characteristic

chemical shifts of the umpolung linkage – [C(Me)=CH–CH<sub>2</sub>–CH(Me)]– appear at δ 139.4, 129.1, 38.62, 32.36, 16.98, and 12.47 ppm. According to the assignments of <sup>1</sup>H NMR spectrum and correlation of <sup>1</sup>H–<sup>13</sup>C HMQC NMR spectra (Figure S18), all resonances in the <sup>13</sup>C NMR spectrum of PIDMA were finally assigned.

Thermal properties of the unsaturated polyesters were examined by differential scanning calorimetry (DSC) and thermal gravimetric analysis (TGA) analyses. DSC curves obtained from the second scan were overlaid in Figure 9,

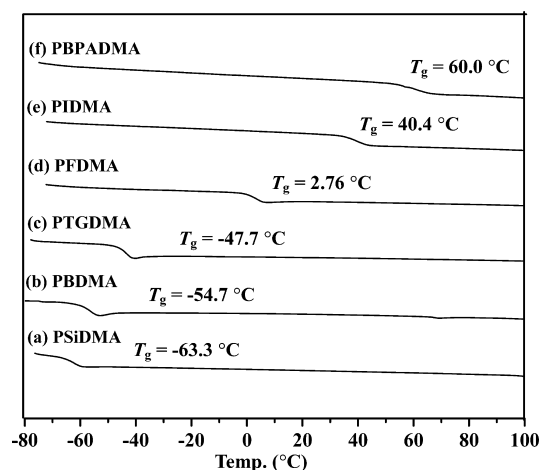
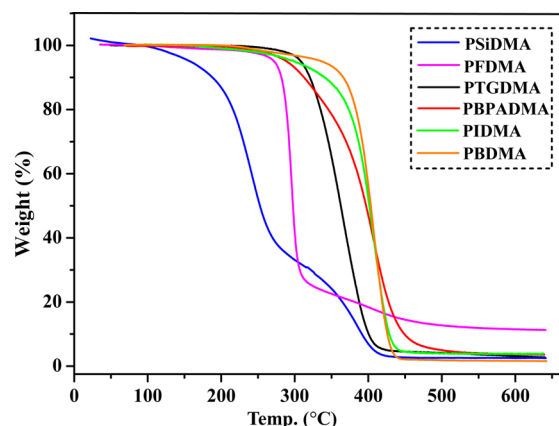


Figure 9. DSC curves of the unsaturated polyesters: (a) PSiDMA (run 4, Table 2), (b) PBDMA (run 1, Table 2), (c) PTGDMA (run 5, Table 2), (d) PFDMA (run 8, Table 2), (e) PIDMA (run 11, Table 2), (f) PBPADMA (run 12, Table 2).

showing the glass transition temperatures ( $T_g$ ) in a wide range from –63.3 to 60 °C, depending on the linker. As anticipated, the  $T_g$  increases with an increase in the rigidity of the main chain, following the order: PSiDMA (–63.3 °C) < PBDMA (–54.7 °C) < PTGDMA (–47.7 °C) < PFDMA (2.76 °C) < PIDMA (40.4 °C) < PBPADMA (60.0 °C). Thus, PBPADMA with the most rigid main chain exhibits the highest  $T_g$  of 60 °C, while PSiDMA with the most flexible main chain displays the lowest  $T_g$  of –63.3 °C. No melting transitions were detected under current DSC conditions, contributable to the disruption of the polyester crystallization by the double bond segment on the main chain.

TGA curves of the unsaturated polyesters were provided in Figure 10. Except PSiDMA which showed low thermal stability



**Figure 10.** TGA curves for PSiDMA ( $T_d = 134.2$  °C,  $T_{max1} = 240.1$  °C,  $T_{max2} = 383.0$  °C, run 4, Table 2), PBDMA ( $T_d = 336.8$  °C,  $T_{max} = 407.7$  °C, run 1, Table 2), PTGDMA ( $T_d = 307.9$  °C,  $T_{max} = 365.9$  °C, run 5, Table 2), PFDMA ( $T_d = 270.0$  °C,  $T_{max} = 296.0$  °C, run 8, Table 2), PIDMA ( $T_d = 293.3$  °C,  $T_{max} = 409.1$  °C, run 11, Table 2), PBPADMA ( $T_d = 290.4$  °C,  $T_{max} = 410.0$  °C, run 12, Table 2).

( $T_d = 134.2$  °C,  $T_d$  defined by the temperature of 5% weight loss in the TGA curve) with a two-step degradation profile, all other polyesters exhibited high thermal stability showing one-step degradation profiles with high  $T_d$ 's ranging from 290 to 308 °C and high maximum degradation temperatures ( $T_{max}$ ) measured by the derivative TGA curves) ranging from 296 to 410 °C (Figure 10). Judged by the relative  $T_d$  values, the thermal stability of the current six unsaturated polyesters follows this trend: PSiDMA < PFDMA < PBPADMA < PIDMA < PTGDMA < PBDMA.

**Unique Properties of PFDMA.** Behaving differently from other unsaturated polyesters that thermally decomposed completely without leaving any residue at >500 °C, PFDMA yielded ~10 wt % residue at temperatures as high as 650 °C, attributable to the formation of stable carbonaceous materials from high temperature treatment of the furfuryl or furan-containing polymers.<sup>54</sup> Another interesting property of PFDMA is the ability to undergo *self-curing* via various cross-linking approaches to produce more robust polyester materials.

PFDMA is stable as long as being kept in solution. However, self-cross-linking of PFDMA occurred readily as soon as the solvent was removed. Even during drying under vacuum, self-cross-linking was observed. In this context, three different approaches to form cross-linked PFDMA were examined: thermally induced, microwave-induced, and Lewis acid-catalyzed cross-linking. Generally, the  $T_g$  value enhances with increasing the degree of cross-linking and, therefore, the observed change of the  $T_g$  of cross-linked PFDMA was used as an indicator to measure the degree of cross-linking. The PFDMA via thermally induced cross-linking after heating at 150 °C for 1 h exhibited a  $T_g$  of 10.6 °C, which is higher than that via microwave-induced cross-linking (4.83 and 8.00 °C) with microwave irradiation (MI) at 25 °C (1500W, 1 and 3 h) and that via vacuum drying (2.72 °C). TGA measurements of the resulting products (Figure 11) showed that the cross-linked PFDMA prepared by thermally ( $T_d = 233.0$  °C) and microwave ( $T_d = 231.0$ – $234.5$  °C) induced cross-linking approaches exhibited lower thermal stability compared with

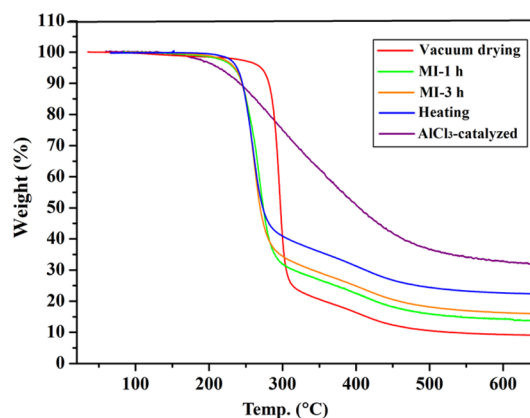


**Figure 11.** TGA curves of cross-linked PFDMA prepared by different approaches: by vacuum drying,  $T_d = 270$  °C, residue = 9.3 wt %; by microwave irradiation (MI) at 25 °C for 1 h (MI-1 h),  $T_d = 231$  °C, residue = 15.9 wt %; by MI at 25 °C for 3 h (MI-3 h),  $T_d = 235$  °C, residue = 20.5 wt %; by heating at 150 °C for 1 h,  $T_d = 233$  °C, residue = 22.2 wt %; by  $AlCl_3$ -catalysis,  $T_d = 213$  °C, residue = 31.4 wt %.

the cross-linked polymer prepared by vacuum drying ( $T_d = 270.0$  °C). Noteworthy here is that the amount of the stable carbonaceous residue formed at 650 °C increased with increasing the degree of cross-linking. Hence, the cross-linked PFDMA after heating at 150 °C for 1 h yielded a high residue amount of 22.2 wt % formed at 650 °C.

Scheme 3 shows the proposed mechanism for the self-cross-linking of PFDMA that proceeds through the Diels–Alder reaction in which the furan rings act as the diene source and the unsaturated double bonds act as the dienophile. To provide evidence supporting this pathway, the hydrogenation reaction of PFDMA over Pd/C was carried out to convert the uncross-linked, unsaturated PFDMA into the corresponding saturated polyester.<sup>30</sup>  $^1H$  NMR spectra of the unsaturated PFDMA and saturated polyester before and after the selective hydrogenation are shown in Figure 12. The most significant change in chemical shifts after the hydrogenation reaction is the complete disappearance of the signal at  $\delta$  6.7 ppm for the double bond (marked as H6). Behaving differently from the unsaturated PFDMA, the obtained saturated polyester had good solubility after removing the solvent or heating and showed no sign of cross-linking. Hence, the inertness of the furan-containing saturated polyester toward cross-linking under identical conditions was used to confirm the self-cross-linking that proceeds through the Diels–Alder reaction as depicted in Scheme 3.

The third approach we investigated is the Lewis acid ( $AlCl_3$ )-catalyzed Diels–Alder reaction in solution, which was employed to further enhance the degree of PFDMA self-cross-linking. FT-IR spectrum (Figure S21) of the cross-linked PFDMA by this method exhibited considerably broader absorption bands compared with PFDMA. In addition, the intensity of the absorption bands attributed to the bending vibration modes of the furan rings at 930 and 736  $cm^{-1}$  noticeably decreased. Furthermore, there was no apparent  $T_g$  observed for the cross-linked PFDMA by this route, and both endothermic and exothermic peaks due to the thermally reversible Diels–Alder reaction were also not observed in DSC curves. Lastly, the cross-linked PFDMA prepared using the  $AlCl_3$ -catalyzed Diels–Alder reaction exhibited a  $T_d$  of 213 °C and a  $T_{max}$  of 315 °C, but it produced the highest amount of the stable carbonaceous residue (31.4 wt %) formed at 650 °C



Scheme 3. Proposed Mechanism for Self-Crosslinking of PFDMA through the Diels–Alder Reaction and the Inertness of the Saturated Polyester toward Such Crosslinking

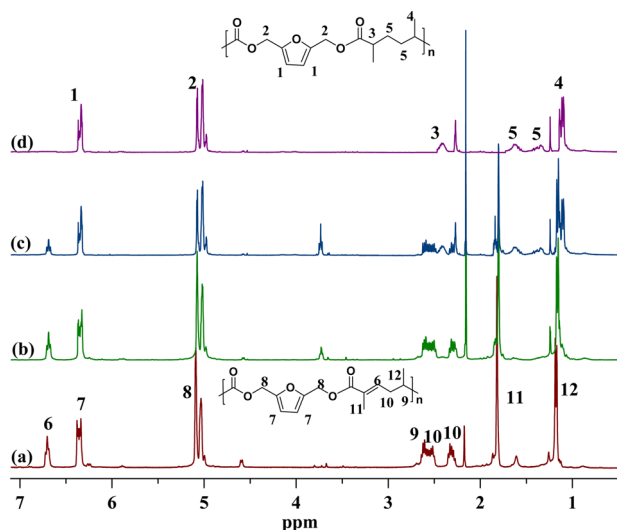
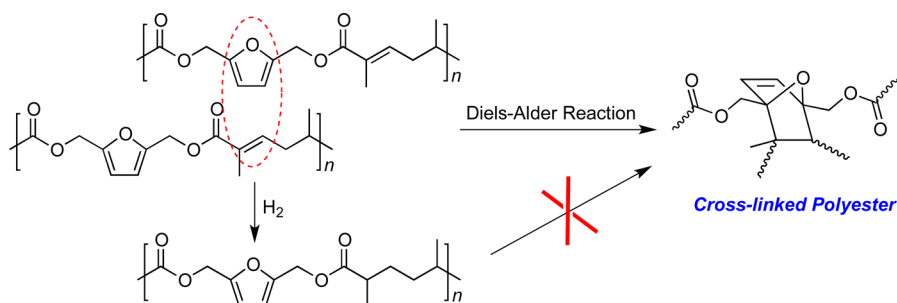


**Figure 12.**  $^1\text{H}$  NMR spectra ( $\text{CDCl}_3$ ) monitoring the hydrogenation reaction: (a) PFDMA (run 8, Table 2), (b) hydrogenation for 6 h (conv. = 15.3%), (c) hydrogenation for 24 h (conv. = 41.2%), and (d) hydrogenation for 48 h (conv. = 100%).

(Figure 11). All together, the above results indicated the higher degree of the cross-linking between the furan rings and unsaturated double bonds of PFDMA achieved via the  $\text{AlCl}_3$ -catalyzed Diels–Alder reaction.

**Effects of TPT Catalysts.** To examine the effects of catalyst structure on the HTP activity, the formation of the bis(enamine) intermediates and resulting polyesters was initially carried out in J. Young-type NMR tubes and monitored by  $^1\text{H}$  NMR. The conversion data for the bis(enamine) formation reaction of BDMA and NHC (2 equiv) in toluene- $d_8$  at 25 °C are summarized in Table S1. The reactivity trend follows the order of  $\text{TPT} < {}^{\text{OMe}^3}\text{TPT} < {}^{\text{OMe}^2}\text{TPT}$ , indicating

that more nucleophilic NHCs with electron-donating substituents enhance the rate of the enamine intermediate formation. In the case of the NMR scale polymerization in a ratio of BDMA/NHC/MP = 5/1/0.1 performed at 80 °C, the reactivity order was somewhat different:  ${}^{\text{OMe}^3}\text{TPT} < \text{TPT} < {}^{\text{OMe}^2}\text{TPT}$ , suggesting that the more nucleophilic NHC is not necessarily a better catalyst for HTP due to its higher resistance toward its release at the end of the propagation cycle (i.e., the poorer leaving group). Hence, a fine balance must be struck between the ability to attack the substrate and the propensity to release from the product, and it appears that  ${}^{\text{OMe}^2}\text{TPT}$  is both a good nucleophile and leaving group.

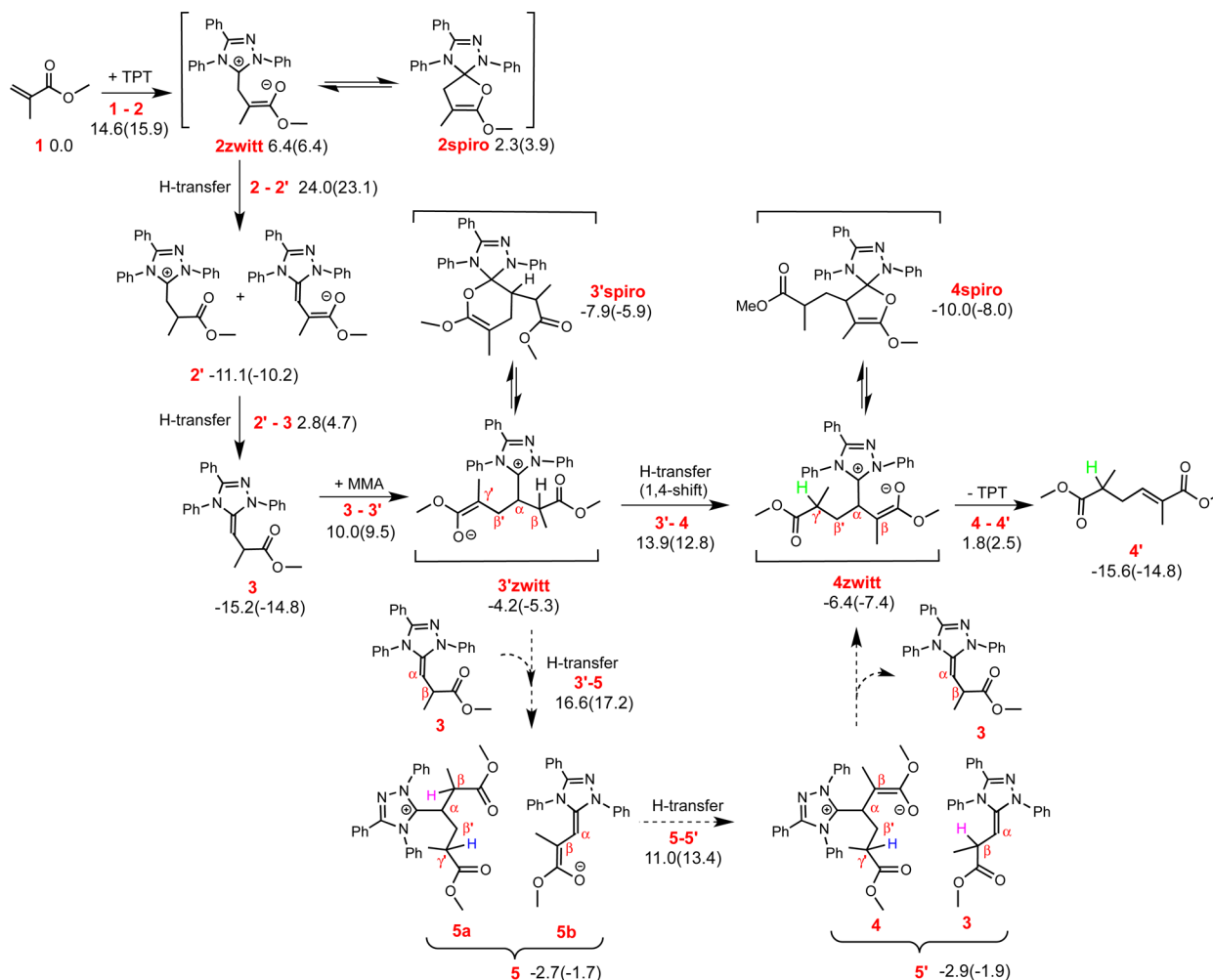
As we showed previously, the direct use of TPT(MeO/H) (1 mol %) for the polymerization of BDMA in the presence of MP (0.1 mol %) in toluene at 100 °C, under which conditions the precatalyst releases the free carbene as the catalyst, led to a similar polymerization performance to that by the free carbene TPT.<sup>51</sup> Using this strategy, precatalysts  ${}^{\text{Cl}^3}\text{TPT}(\text{MeO}/\text{H})$  and  ${}^{\text{Cl}^2}\text{TPT}(\text{MeO}/\text{H})$  were used for their HTP studies as their free carbene forms are unstable under the current reaction conditions in the absence of monomer. In comparison, these Cl-substituted TPT derivatives are considerably less active than the parent TPT (Table S1), indicating that electron-withdrawing groups on TPT decrease the HTP activity.

The polymerization results obtained from the preparative scale polymerization runs are summarized in Table 3. Relative to TPT (1 mol %), which achieved quantitative monomer conversion in the BDMA polymerization (BDMA/TPT/MP = 100/1/0.1) at 100 °C after 48 h and produced PBDMA with  $M_n = 14.2$  kg/mol and  $\bar{D} = 1.70$  (run 1, Table 3),  ${}^{\text{OMe}^2}\text{TPT}$  exhibited higher activity under identical conditions, thus shortening the time to reach the quantitative monomer conversion by more than a half (20 h) and also producing PBDMA with a higher  $M_n$  of 16.7 kg/mol and a lower  $\bar{D}$  value of 1.64 (run 2, Table 3). On the other hand, the TPT derivative

**Table 3.** Results of HTP of BDMA by TPT and MeO- and Cl-Substituted TPT Derivatives<sup>a</sup>

Run	(pre)catalyst	BDMA/NHC/MP	Temp. (°C)	Time (h)	Conv. (%) <sup>b</sup>	$M_n^c$ (kg/mol)	$\bar{D}^c$ ( $M_w/M_n$ )
1	TPT	100/1/0.1	100	48	100	14.2	1.70
2	${}^{\text{OMe}^2}\text{TPT}$	100/1/0.1	100	20	100	16.7	1.64
3	${}^{\text{OMe}^3}\text{TPT}$	20/1/0.02	80	12	100	14.0	1.60
4	${}^{\text{OMe}^3}\text{TPT}$	100/1/0.1	110	24	86.0	8.36	1.15
5	${}^{\text{Cl}^2}\text{TPT}(\text{MeO}/\text{H})$	20/1/0.1	110	10	99.1	11.5	1.40
6	${}^{\text{Cl}^3}\text{TPT}(\text{MeO}/\text{H})$	20/1/0.1	110	10	99.2	16.6	1.52
7	${}^{\text{Cl}^3}\text{TPT}(\text{MeO}/\text{H})$	100/1/0.1	110	48	75.0	7.15	1.10

<sup>a</sup>Conditions:  $[\text{BDMA}] = 1.6$  M in toluene. <sup>b</sup>Conv.% = monomer conversion measured by  $^1\text{H}$  NMR spectroscopy. <sup>c</sup> $M_n$  and  $\bar{D}$  determined by GPC at 40 °C in DMF relative to PMMA standards.

Scheme 4. Schematic Representation of the HTP Chain Growth Step<sup>a</sup>

<sup>a</sup>Free energies (kcal/mol) reported in both toluene and DMF (in parentheses).

with three MeO substituents, <sup>OMe</sup>3-TPT, is less active and effective as compared with TPT and can achieve quantitative monomer conversion only with a relatively high catalyst loading of 5 mol % in 10 h (run 3, Table 3); with a lower catalyst loading of 1 mol % (BDMA/<sup>OMe</sup>3-TPT/MP = 100/1/0.1), the polymerization achieved only 86% monomer conversion after 24 h even when the temperature was raised to 110 °C and produced the PBDMA with a lower molecular weight (run 4, Table 3). Consistent with the reactivity results obtained by the NMR monitoring of the polymerization, the preparative scale polymerization results showed that the Cl-substituted TPT derivatives, <sup>Cl</sup>3-TPT(MeO/H) and <sup>Cl</sup>2-TPT(MeO/H), are the least active and effective NHC catalysts within the series examined herein; they can achieve high monomer conversions only with a relatively high catalyst loading of 5 mol % (runs 5 and 6, Table 3), but when the catalyst loading was lowered to 1 mol % the activity of the polymerization by <sup>Cl</sup>3-TPT (MeO/H) decreased drastically, with a conversion of only 75.0% even after 48 h and also produced the PBDMA product with a relatively low  $M_n$  of 7.15 kg/mol (run 7, Table 3).

**Theoretical Investigation of the HTP Mechanism.** In this section we describe the mechanism of the condensation coupling step in the TPT-catalyzed DMA polymerization. As a suitable model for the propagation cycle outlined in Scheme 2, we investigated the tail-to-tail dimerization of MMA in detail.

The entire dimerization pathway mechanism is reported in Scheme 4. It should be noted that steps 1 to 3', corresponding to the initial attack of TPT to a free methacrylate unit toward formation of the enamine intermediate 3, and the following attack of 3 to a second methacrylate unit, were discussed previously.<sup>33</sup> As we have improved the level of theory on which these calculations are performed from internal energies at the BP86 level to free energies at the M06 level, for the sake of consistency we briefly rediscuss steps 1 to 3' here.

The first step, from 1 to 2, corresponds to the nucleophilic attack of TPT to the C=C double bond of a MMA molecule mimicking one of the methacrylate moieties of DMA. Further evolution of 2 occurs via a double H-transfer between two molecules of 2 via ion-pair intermediate 2', leading to the formation of two molecules of enamine 3 with free energy barriers around 15 kcal/mol. Formation of 3, roughly 15 kcal/mol below the starting species 1, both in toluene and in DMF, is clearly exergonic. Nucleophilic attack of 3 to the C=C double bond of a free MMA molecule, via transition state 3-3' with an energy barrier around 25 kcal/mol, leads to intermediate 3', roughly 10 kcal/mol above 3. The novel feature of the current investigation is the inclusion of spirocyclic structures for 2 and 3'; in both cases, the spirocyclic structure is more stable than the open-chain zwitterionic structure by less than 5 kcal/mol, indicating an overall equilibrium between

them. Even with the addition of the spirocyclic structures, the overall chemical scenario for the conversion of **1** to **3'** depicted here, using M06 free energies, confirms the conclusions drawn on the basis of BP86 internal energies.<sup>33</sup>

Evolution of intermediate **3'** toward the dimerization product **4'** has been studied via two different pathways (Scheme 4). The first is the proposed 1,4-shift of the H atom from the *C $\beta$*  to the *C $\gamma$ '* through five-membered transition state **3'-4** as depicted in Figure 13, with a barrier of about 18–20

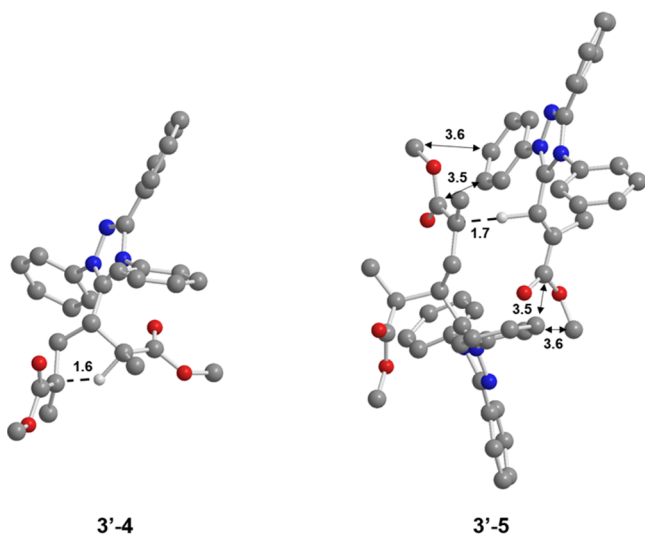


Figure 13. Geometries of transition states **3'-4** and **3'-5**. Marked distances in Å.

kcal/mol in both solvents (and an overall energy cost of about 28–30 kcal/mol from the most stable intermediate **3**). The resulting intermediate **4**, roughly 2 kcal/mol lower in energy than **3'**, undergoes NHC dissociation through transition state **4-4'**, around 10–12 kcal/mol lower in energy than transition state **3'-4**, leading to the dimerization product **4'** and release of TPT. The overall transformation from **3** to **4'** is basically thermoneutral in both toluene and DMF. The second pathway

considered corresponds to a two-step bimolecular H-transfer reaction involving **3'** and one molecule of enamine **3**. In the first step, one H atom (colored in blue in Scheme 4) is transferred from the *C $\beta$*  of **3** to the *C $\gamma$ '* of **3'**, through transition state **3'-5** and an energy barrier of roughly 21 kcal/mol in both solvents, leading to the formation of the ion pair intermediate **5**. To complete the tail-to-tail condensation step, intermediate **5** undergoes a further H-transfer reaction through transition state **5-5'**, where one H atom is transferred from the *C $\beta$*  of the **5a** moiety to the *C $\beta$*  of the **5b** moiety, leading to **4** plus **3**. Transition state **5-5'** is around 4–5 kcal/mol lower in energy than transition state **3'-5**, and the overall step **5** to **5'** is thermoneutral. As in the intramolecular mechanism depicted above, **4** undergoes TPT dissociation leading to the condensation product **4'**.

Comparing the two mechanisms depicted in Scheme 4 for the conversion of **3'** to **4**, evolution of **3'** through transition state **3'-4** is favored over evolution through transition state **3'-5**, since transition state **3'-4** is roughly 3–5 kcal/mol lower in energy relative to transition state **3'-5**.<sup>55</sup> The geometries of the pathway determining transition states **3'-4** and **3'-5** are compared in Figure 13. The unimolecular transition state **3'-4** shows the H atom moving from the *C $\beta$*  to the *C $\gamma$ '* within an unstrained five-membered ring transition state. In contrast, the bimolecular transition state **3'-5** shows a much more crowded geometry, with substituents on both TPT units clashing with the MMA skeleton of the other adduct, as indicated by the short C–C distances in Figure 13. The final favored energy profile involving both spiro and zwitterionic species is depicted in Figure 14.

**Mechanistic Scenario with Spirocycle Structures: TPT vs IMes.** In our efforts to find the possible theoretical basis to explain why so far only the triazolylidene carbene TPT promotes the above HTP reaction while the imidazolylidene carbenes such as IMes fail to catalyze the same reaction, we focused on the intermediates along the dimerization pathway (*i.e.* species **2**, **3'** and **4**, Scheme 4). As anticipated above, we found they can exist as both open zwitterionic and closed spirocyclic structures.<sup>7e</sup> The zwitterionic species are expected to have the positive charge mainly localized on the NHC and the

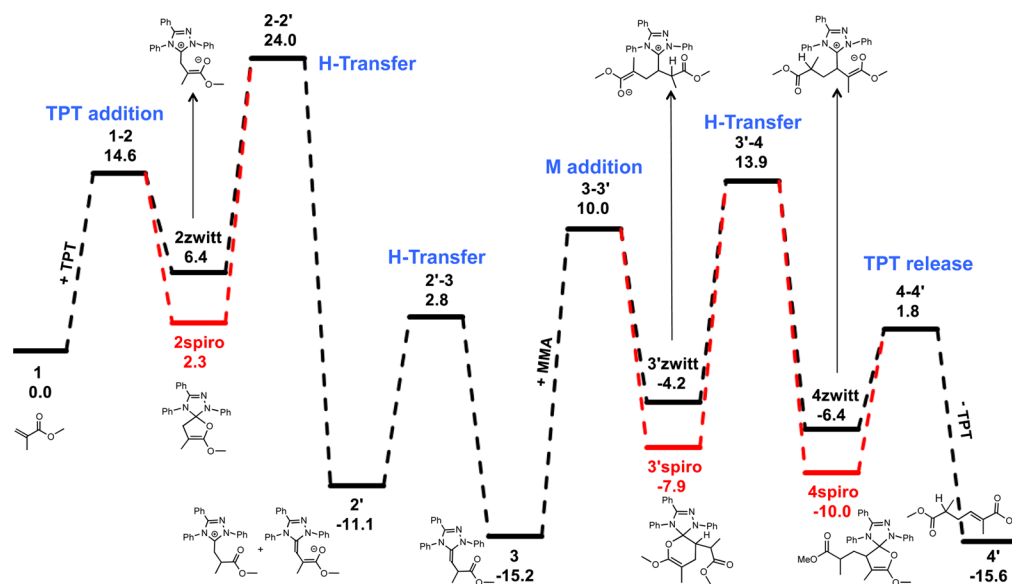
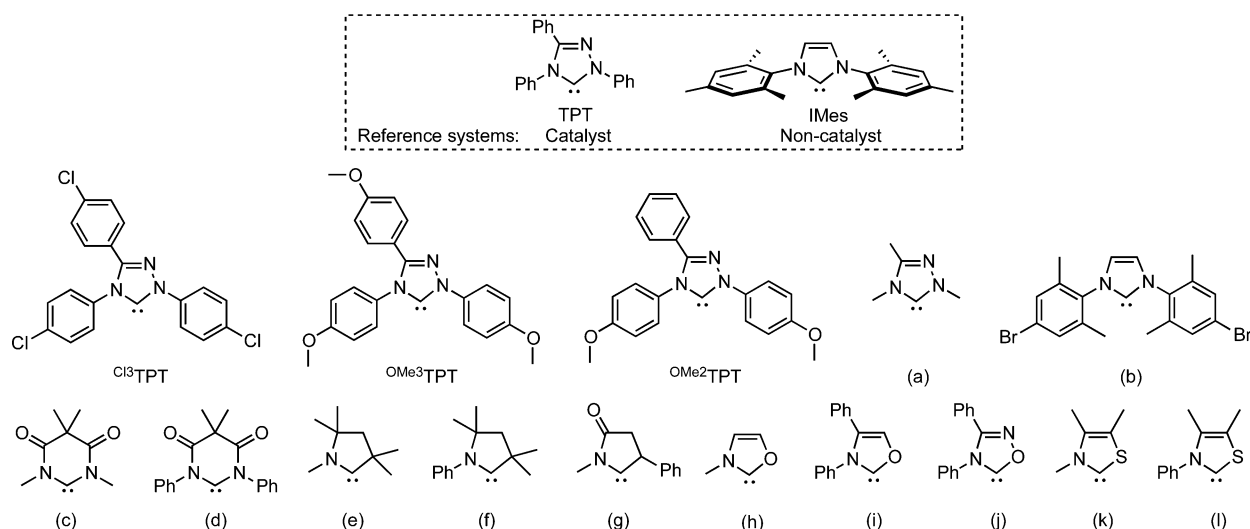


Figure 14. Energy profile of the HTP chain growth step. Free energies (kcal/mol) are reported in toluene.

Chart 1. NHC Structures Screened Computationally for Their Suitability as a Catalyst for HTP



negative charge delocalized on the chain, while the spirocyclic species have no formal charge separation. Given this chief difference, the relative stability of the zwitterionic and spirocyclic structures depends on the solvent polarity, with more polar solvents favoring the zwitterionic form. In line with the above reasoning, we found that the spirocyclic forms of **2**, **3'** and **4** are around 4 kcal/mol more stable than the corresponding zwitterionic forms in toluene, but this difference is reduced to 1–2 kcal/mol in DMF. As the key intermediate along the dimerization pathway, from which the coupling with another poly-DMA chain end starts, **3'** is remarkably unstable in its open zwitterionic form over the proceeding enamine species **3**, which prevents formation of a sizable amount of **3'**. Hence, we speculated that formation of a more stable spirocyclic structure for **3'** could drive thermodynamically the reaction toward the polymerization products.

To test this hypothesis, we endeavored to locate analogous intermediates derived from IMes, an NHC unable to promote HTP. Interestingly, we were not able to locate a spirocyclic geometry for **3'** with IMes as the NHC. Consistently with an open zwitterionic geometry, in all the cases the NHC...O distance converges to the high value of 2.7 Å, versus a value of 1.5 Å in the spirocyclic form of **3'** with TPT. Comparing the relative energy (in toluene) of the most stable geometry of **3** and **3'** derived from IMes and TPT, –19.1 and 1.9 kcal/mol vs –15.2 and –7.9 kcal/mol, it emerges that **3** is roughly 21 kcal/mol more stable than **3'-zwitterion** for IMes, whereas this difference is reduced to about 7 kcal/mol only for TPT, due to the formation of the stable **3'-spiro** species. These results account for the experimental formation of the enamine **3** with IMes, while with TPT the reaction evolves to the dimerization product **4** under the same experimental conditions. Overall, these results suggest that the different behavior between IMes and TPT is not due to kinetics (the rate-determining step, with a barrier of 24–25 kcal/mol, is similar for the two NHC-based systems). Rather, it is due to thermodynamic accessibility of the key intermediate **3'**, which is highly disfavored with IMes, while it can be formed with TPT via a stable spirocycle.

Based on the above knowledge, we explored computationally a series of NHC structures to search for NHCs other than TPT, which are capable of promoting HTP. The two main guidelines in this screening were the following. First, sterically

demanding and rigid NHCs were excluded, since they were shown to exhibit too high energy barriers to promote the bimolecular 2–2' and 2'–3 H transfer steps.<sup>33</sup> Second, we focused on the relative stabilities of **2**, **3**, **3'**, **4** and **4'** and, among the different NHCs tested, we initially selected the systems showing high stability of **3'** and **4** relative to the enamine **3**. Finally, the key transition state 3–3' was located for the most promising NHCs. The NHCs we examined are reported in Chart 1, while the energies of the key intermediates are included in Table S5 of the SI. This screening indicated Cl<sub>3</sub>TPT, OMe<sub>3</sub>TPT, OMe<sub>2</sub>TPT and NHC-(h) as promising catalysts, since they showed a behavior close or even better than that of the parent TPT system. In fact, for these NHCs the spirocyclic form of **3'** is quite stable compared to the enamine intermediate **3**, and the key energy barrier for the **3** to **3'** transformation is comparable to that obtained with TPT for Cl<sub>3</sub>TPT, OMe<sub>3</sub>TPT, and OMe<sub>2</sub>TPT (around 25 kcal/mol) and even lower for NHC-(h) (around 20 kcal/mol). As described above, Cl<sub>3</sub>TPT, OMe<sub>3</sub>TPT, and OMe<sub>2</sub>TPT are indeed competent catalysts to promote HTP, with OMe<sub>2</sub>TPT being the most active and effective (i.e., even better than TPT).

## CONCLUSIONS

The current NHC-catalyzed HTP of acrylic monomers into unsaturated polyesters departs from both the conventional HTP processes and acrylic polymerization systems in two key fronts. First, unlike the typical HTP process, which relies on transfer of protons from the protic group contained in or originated from the monomer, the current HTP deals with acrylic monomers containing no protic groups but relies on the umpolung mechanism that enables the proton-transfer process for coupling of the two electrophiles. Second, unlike the typical acrylic polymerization system that produces nonbiodegradable polyacrylates through polyadditions across C=C double bonds, this NHC-catalyzed HTP converts acrylic monomers into degradable unsaturated polyesters through the umpolung condensation coupling via proton transfer and the step-growth propagation cycles via enamine intermediates, consisting of the repeated conjugate addition–proton transfer–NHC release fundamental steps.

To examine the monomer scope, dimethacrylates having six different types of linkages connecting the two methacrylate

moieties have been employed for TPT-catalyzed HTP studies and found that all of the DMAs can be effectively polymerized into the corresponding unsaturated polyesters. The polymerization activity correlates with increasing the electron deficiency of the methacrylate double bond and the rigidity of the DMA structure, following the increasing order: SiDMA < BDMA  $\approx$  FDMA < TGDMA  $\approx$  BPADMA < IDMA, and the  $T_g$  of the resulting unsaturated polyesters increases with an increase in the rigidity of the main chain: PSiDMA ( $-63.3$  °C) < PBDMA ( $-54.7$  °C) < PTGDMA ( $-47.7$  °C) < PFDMA (2.76) < PIDMA (40.4 °C) < PBPADMA (60.0 °C). Judged by the relative  $T_d$  values, the thermal stability of the current six unsaturated polyesters follows this trend: PSiDMA < PFDMA < PBPADMA < PIDMA < PTGDMA < PBDMA. The HTP of BDMA gave the polymer with the highest molecular weight ( $M_n = 15.8$  kg/mol,  $D = 1.73$ ) and thermal stability ( $T_d = 336.8$  °C,  $T_{max} = 407.7$  °C).

Among the six types of the unsaturated polyesters produced by the current HTP, PFDMA based on the biomass-derived monomer is most unique in two key aspects. First, while other unsaturated polyesters can be decomposed completely without leaving any residue at  $>500$  °C, PFDMA yielded  $\sim 10$  wt % residue as stable carbonaceous materials) at 650 °C. Second, possessing both the diene (the furan ring) and dienophile (the double bond), PFDMA can undergo Diels–Alder reaction-based self-curing via three routes to produce more robust polyester materials, including thermally induced, microwave-induced, and Lewis acid-catalyzed cross-linking. The  $AlCl_3$ -catalyzed Diels–Alder reaction produced the material with the highest degree of cross-linking and also the largest amount of the stable carbonaceous residue formed at 650 °C (31.4 wt %).

To investigate the effects of the catalyst structure on HTP, we have synthesized four new MeO- and Cl-substituted TPT derivatives as methanol insertion products (or precatalysts),  $R^xTPT(MeO/H)$  ( $R = MeO, Cl; x = 2, 3$ ), and two free carbenes (or catalysts),  $^{OMe2}TPT$  and  $^{OMe3}TPT$ , as well as structurally characterized  $^{OMe2}TPT(MeO/H)$  and  $^{OMe2}TPT$ . The structure/reactivity relationship study revealed that the more nucleophilic NHC with electron-donating substituents ( $^{OMe3}TPT$  and  $^{OMe2}TPT$ ) exhibits higher rates for the enamine intermediate formation, but in the case of polymerization activity, the more nucleophilic NHC (thus the poorer leaving group) is not necessarily a better catalyst for HTP due to its higher resistance toward its release at the end of the propagation cycle. Within this series of NHC catalysts investigated,  $^{OMe2}TPT$  exhibited the highest HTP activity and also produced the polyester with the highest molecular weight ( $M_n = 16.7$  kg/mol,  $D = 1.64$ ), attributable to this NHC being both a strong nucleophile and a good leaving group. On the other hand, the TPT derivative with three MeO substituents ( $^{OMe3}TPT$ ) is less active and effective as compared with TPT. Moreover, Cl-substituted TPT derivatives are considerably less active than the parent TPT, indicating that electron-withdrawing groups on TPT decrease the HTP activity.

Theoretical investigation of the HTP mechanism revealed that, after the nucleophilic attack of the second monomer molecule by the enamine intermediate derived from the first monomer addition step, the subsequent key H-transfer step follows an intramolecular mechanism via a five-membered transition state (thus formally 1,4-H shift). The zwitterionic intermediates along the dimerization pathway can adopt the more stable closed spirocyclic structures. On the base of the relative energies, we proposed that formation of more stable

spirocyclic structures for TPT drives thermodynamically the reaction toward the polymerization products. Based on this knowledge, computational screening led to several other NHC structures also capable of promoting HTP.

## ■ ASSOCIATED CONTENT

### Supporting Information

The Supporting Information is available free of charge on the ACS Publications website at DOI: 10.1021/jacs.5b13019.

Full experimental and computational details as well as NMR spectra, DSC curves, FT-IR spectra, conversion data, crystal data, bond lengths and angles, internal energies, and Cartesian coordinates. (PDF)

Cif data for  $C_{23}H_{23}N_3O_3$  (CIF)

Cif data for  $C_{22}H_{19}N_3O_2$  (CIF)

## ■ AUTHOR INFORMATION

### Corresponding Authors

\*luigi.cavallo@kaust.edu.sa

\*eugene.chen@colostate.edu

### Notes

The authors declare no competing financial interest.

## ■ ACKNOWLEDGMENTS

This work was supported by the US National Science Foundation (NSF-1300267) for the study carried out at Colorado State University. Luigi Cavallo thanks the HPC team of Enea ([www.enea.it](http://www.enea.it)) for using the ENEA-GRID and the HPC facilities CRESCO ([www.cresco.enea.it](http://www.cresco.enea.it)) in Portici, Italy.

## ■ REFERENCES

- (1) Selected reviews on organopolymerization: (a) Sardon, H.; Pascual, A.; Mecerreyes, D.; Taton, D.; Cramail, H.; Hedrick, J. L. *Macromolecules* **2015**, *48*, 3153–3165. (b) Fuchise, K.; Chen, Y.; Satoh, T.; Kakuchi, T. *Polym. Chem.* **2013**, *4*, 4278–4291. (c) Kiesewetter, M. K.; Shin, E. J.; Hedrick, J. L.; Waymouth, R. M. *Macromolecules* **2010**, *43*, 2093–2107. (d) Kamber, N. E.; Jeong, W.; Waymouth, R. M.; Pratt, R. C.; Lohmeijer, B. G. G.; Hedrick, J. L. *Chem. Rev.* **2007**, *107*, 5813–5840.
- (2) Selected recent reviews on organocatalysis: (a) Volla, C. M. R.; Atodiresei, I.; Rueping, M. *Chem. Rev.* **2014**, *114*, 2390–2431. (b) Liu, D.; Chen, E. Y.-X. *Green Chem.* **2014**, *16*, 964–981. (c) Grondal, C.; Jeanty, M.; Enders, D. *Nat. Chem.* **2010**, *2*, 167–178. (d) Marcelli, T.; Hiemstra, H. *Synthesis* **2010**, *2010*, 1229–1279.
- (3) Selected recent reviews on NHCs and NHC-mediated organic reactions: (a) Flanigan, D. M.; Romanov-Michailidis, F.; White, N. A.; Rovis, T. *Chem. Rev.* **2015**, *115*, 9307–9387. (b) Hopkinson, M. N.; Richter, C.; Schedler, M.; Glorius, F. *Nature* **2014**, *510*, 485–496. (c) Nelson, D. J.; Nolan, S. P. *Chem. Soc. Rev.* **2013**, *42*, 6723–6753. (d) Ryan, S. J.; Candish, L.; Lupton, D. W. *Chem. Soc. Rev.* **2013**, *42*, 4906–4917.
- (4) (a) Nyce, G. W.; Glauser, T.; Connor, E. F.; Möck, A.; Waymouth, R. M.; Hedrick, J. L. *J. Am. Chem. Soc.* **2003**, *125*, 3046–3056. (b) Connor, E. F.; Nyce, G. W.; Myers, M.; Möck, A.; Hedrick, J. L. *J. Am. Chem. Soc.* **2002**, *124*, 914–915. (c) Nederberg, F.; Connor, E. F.; Möller, M.; Glauser, T.; Hedrick, J. L. *Angew. Chem., Int. Ed.* **2001**, *40*, 2712–2715.
- (5) Selected reviews on NHC-mediated organopolymerization: (a) Matsuoka, S.-I. *Polym. J.* **2015**, *47*, 713–718. (b) Naumann, S.; Dove, A. P. *Polym. Chem.* **2015**, *6*, 3185–3200. (c) Naumann, S.; Buchmeiser, M. R. *Catal. Sci. Technol.* **2014**, *4*, 2466–2479. (d) Fèvre, M.; Pinaud, J.; Gnanou, Y.; Vignolle, J.; Taton, D. *Chem. Soc. Rev.* **2013**, *42*, 2142–2172.
- (6) (a) Jeong, W.; Shin, E. J.; Culkun, D. A.; Hedrick, J. L.; Waymouth, R. M. *J. Am. Chem. Soc.* **2009**, *131*, 4884–4891. (b) Culkun,

- D. A.; Jeong, W.; Csihony, S.; Gomez, E. D.; Balsara, N. P.; Hedrick, J. L.; Waymouth, R. M. *Angew. Chem., Int. Ed.* **2007**, *46*, 2627–2630.
- (c) Dove, A. P.; Li, H.; Pratt, R. C.; Lohmeijer, B. G. G.; Culkun, D. A.; Waymouth, R. M.; Hedrick, J. L. *Chem. Commun.* **2006**, 2881–2883.
- (d) Coulembier, O.; Dove, A. P.; Pratt, R. C.; Sentman, A. C.; Culkun, D. A.; Mespouille, L.; Dubois, P.; Waymouth, R. M.; Hedrick, J. L. *Angew. Chem., Int. Ed.* **2005**, *44*, 4964–4968.
- (e) Csihony, S.; Culkun, D. A.; Sentman, A. C.; Dove, A. P.; Waymouth, R. M.; Hedrick, J. L. *J. Am. Chem. Soc.* **2005**, *127*, 9079–9084.
- (7) (a) Brown, H. A.; Xiong, S.; Medvedev, G.; Chang, Y. A.; Abu-Omar, M. M.; Caruthers, J. M.; Waymouth, R. M. *Macromolecules* **2014**, *47*, 2955–2963. (b) Shin, E. J.; Brown, H. A.; Gonzalez, S.; Jeong, W.; Hedrick, J. L.; Waymouth, R. M. *Angew. Chem., Int. Ed.* **2011**, *50*, 6388–6391. (c) Sen, T. K.; Sau, S.; Ch.; Mukherjee, A.; Modak, A.; Mandal, S. K.; Koley, D. *Chem. Commun.* **2011**, *47*, 11972–11974. (d) Kamber, N. E.; Jeong, W.; Gonzalez, S.; Hedrick, J. L.; Waymouth, R. M. *Macromolecules* **2009**, *42*, 1634–1639. (e) Jeong, W.; Hedrick, J. L.; Waymouth, R. M. *J. Am. Chem. Soc.* **2007**, *129*, 8414–8415.
- (8) (a) Raynaud, J.; Absalon, C.; Gnanou, Y.; Taton, D. *Macromolecules* **2010**, *43*, 2814–2823. (b) Raynaud, J.; Ottou, W. N.; Gnanou, Y.; Taton, D. *Chem. Commun.* **2010**, *46*, 3203–3205. (c) Raynaud, J.; Absalon, C.; Gnanou, Y.; Taton, D. *J. Am. Chem. Soc.* **2009**, *131*, 3201–3209.
- (9) Nederberg, F.; Lohmeijer, B. G. G.; Leibfarth, F.; Pratt, R. C.; Choi, J.; Dove, A. P.; Waymouth, R. M.; Hedrick, J. L. *Biomacromolecules* **2007**, *8*, 153–160.
- (10) (a) Brown, H. A.; Chang, Y. A.; Waymouth, R. M. *J. Am. Chem. Soc.* **2013**, *135*, 18738–18941. (b) Rodriguez, M.; Marrot, S.; Kato, T.; Stérin, S.; Fleury, E.; Baceiredo, A. J. *Organomet. Chem.* **2007**, *692*, 705–708. (c) Lohmeijer, B. G. G.; Dubois, G.; Leibfarth, F.; Pratt, R. C.; Nederberg, F.; Nelson, A.; Waymouth, R. M.; Wade, C.; Hedrick, J. L. *Org. Lett.* **2006**, *8*, 4683–4686.
- (11) (a) Guo, L.; Lahasky, S. H.; Ghale, K.; Zhang, D. *J. Am. Chem. Soc.* **2012**, *134*, 9163–9171. (b) Guo, L.; Zhang, D. *J. Am. Chem. Soc.* **2009**, *131*, 18072–18074.
- (12) (a) Coutelier, O.; El Ezzi, M.; Destarac, M.; Bonnette, F.; Kato, T.; Baceiredo, A.; Sivasankarapillai, G.; Gnanou, Y.; Taton, D. *Polym. Chem.* **2012**, *3*, 605–608. (b) Pinaud, J.; Vijayakrishna, K.; Taton, D.; Gnanou, Y. *Macromolecules* **2009**, *42*, 4932–4936. (c) Nyce, G. W.; Lamboy, J. A.; Connor, E. F.; Waymouth, R. M.; Hedrick, J. L. *Org. Lett.* **2002**, *4*, 3587–3590.
- (13) (a) Webster, O. W. *Adv. Polym. Sci.* **2003**, *167*, 1–34. (b) Sogah, D. Y.; Hertler, W. R.; Webster, O. W.; Cohen, G. M. *Macromolecules* **1987**, *20*, 1473–1488. (c) Webster, O. W.; Hertler, W. R.; Sogah, D. Y.; Farnham, W. B.; RajanBabu, T. V. *J. Am. Chem. Soc.* **1983**, *105*, 5706–5708.
- (14) (a) Raynaud, J.; Liu, N.; Gnanou, Y.; Taton, D. *Macromolecules* **2010**, *43*, 8853–8861. (b) Raynaud, J.; Gnanou, Y.; Taton, D. *Macromolecules* **2009**, *42*, 5996–6005. (c) Raynaud, J.; Ciolino, A.; Baceiredo, A.; Destarac, M.; Bonnette, F.; Kato, T.; Gnanou, Y.; Taton, D. *Angew. Chem., Int. Ed.* **2008**, *47*, 5390–5393. (d) Scholten, M. D.; Hedrick, J. L.; Waymouth, R. M. *Macromolecules* **2008**, *41*, 7399–7404.
- (15) Selected reviews: (a) Stephan, D. W.; Erker, G. *Angew. Chem., Int. Ed.* **2015**, *54*, 6400–6441. (b) Stephan, D. W.; Erker, G. *Angew. Chem., Int. Ed.* **2010**, *49*, 46–76.
- (16) (a) Arduengo, A. J., III; Bock, H.; Chen, H.; Denk, M.; Dixon, D. A.; Green, J. C.; Herrmann, W. A.; Jones, N. L.; Wagner, M.; West, R. *J. Am. Chem. Soc.* **1994**, *116*, 6641–6649. (b) Arduengo, A. J., III; Dias, H. V. R.; Harlow, R. L.; Kline, M. *J. Am. Chem. Soc.* **1992**, *114*, 5530–5534.
- (17) (a) He, J.; Zhang, Y.; Falivene, L.; Caporaso, L.; Cavallo, L.; Chen, E. Y.-X. *Macromolecules* **2014**, *47*, 7765–7774. (b) He, J.; Zhang, Y.; Chen, E. Y.-X. *Synlett* **2014**, *25*, 1534–1538. (c) Chen, E. Y.-X. *Top. Curr. Chem.* **2012**, *334*, 239–260. (d) Zhang, Y.; Miyake, G. M.; John, M. G.; Falivene, L.; Caporaso, L.; Cavallo, L.; Chen, E. Y.-X. *Dalton Trans.* **2012**, *41*, 9119–9134. (e) Zhang, Y.; Miyake, G. M.; Chen, E. Y.-X. *Angew. Chem., Int. Ed.* **2010**, *49*, 10158–10162.
- (18) Fischer, C.; Smith, S. W.; Powell, D. A.; Fu, G. C. *J. Am. Chem. Soc.* **2006**, *128*, 1472–1473.
- (19) (a) Enders, D.; Breuer, K.; Kallfass, U.; Balensiefer, T. *Synthesis* **2003**, 1292–1295. (b) Enders, D.; Breuer, K.; Raabe, G.; Runsink, J.; Teles, J. H.; Melder, J.-P.; Ebel, K.; Brode, S. *Angew. Chem., Int. Ed. Engl.* **1995**, *34*, 1021–1023.
- (20) Zhang, Y.; Chen, E. Y.-X. *Angew. Chem., Int. Ed.* **2012**, *51*, 2465–2469.
- (21) Maji, B.; Breugst, M.; Mayr, H. *Angew. Chem., Int. Ed.* **2011**, *50*, 6915–6919.
- (22) Selected recent work on the structural characterization and properties of the deoxy-Breslow intermediate: (a) Ref 20.. (b) Maji, B.; Horn, M.; Mayr, H. *Angew. Chem., Int. Ed.* **2012**, *51*, 6231–6235. (c) Knappke, C. E. I.; Arduengo, A. J., III; Jiao, H.; Neudörfel, J.-M.; von Wangelin, J. A. *Synthesis* **2011**, *2011*, 3784–3795. (d) Knappke, C. E. I.; Neudörfel, J.-M.; von Wangelin, J. A. *Org. Biomol. Chem.* **2010**, *8*, 1695–1705.
- (23) Selected recent work on the structural characterization and properties of the Breslow intermediate: (a) Berkessel, A.; Yatham, V. R.; Elfert, S.; Neudörfel, J.-M. *Angew. Chem., Int. Ed.* **2013**, *52*, 11158–11162. (b) Maji, B.; Mayr, H. *Angew. Chem., Int. Ed.* **2013**, *52*, 11163–11167. (c) Liu, D.; Chen, E. Y.-X. *ChemSusChem* **2013**, *6*, 2236–2239. (d) Berkessel, A.; Elfert, S.; Yatham, V. R.; Neudörfel, J.-M.; Schlörner, N. E.; Teles, J. H. *Angew. Chem., Int. Ed.* **2012**, *51*, 12370–12374. (e) DiRocco, D. A.; Oberg, K. M.; Rovis, T. *J. Am. Chem. Soc.* **2012**, *134*, 6143–6145. (f) Maji, B.; Mayr, H. *Angew. Chem., Int. Ed.* **2012**, *51*, 10408–10412. (g) Berkessel, A.; Elfert, S.; Etzenbach-Effers, K.; Teles, J. H. *Angew. Chem., Int. Ed.* **2010**, *49*, 7120–7124.
- (24) (a) Kluger, R.; Tittmann, K. *Chem. Rev.* **2008**, *108*, 1797–1833. (b) Breslow, R. *J. Am. Chem. Soc.* **1958**, *80*, 3719–3726. (c) Breslow, R. *J. Am. Chem. Soc.* **1957**, *79*, 1762–1763.
- (25) Biju, A. T.; Padmanaban, M.; Wurz, N. E.; Glorius, F. *Angew. Chem., Int. Ed.* **2011**, *50*, 8412–8415.
- (26) (a) Kato, T.; Ota, Y.; Matsuoka, S.-I.; Takagi, K.; Suzuki, M. *J. Org. Chem.* **2013**, *78*, 8739–8747. (b) Matsuoka, S.-I.; Ota, Y.; Washio, A.; Katada, A.; Ichioka, K.; Takagi, K.; Suzuki, M. *Org. Lett.* **2011**, *13*, 3722–3725.
- (27) Kato, T.; Matsuoka, S.-I.; Suzuki, M. *J. Org. Chem.* **2014**, *79*, 4484–4491.
- (28) Schedler, M.; Wurz, N. E.; Daniliuc, C. G.; Glorius, F. *Org. Lett.* **2014**, *16*, 3134–3137.
- (29) Matsuoka, S.-I.; Nakazawa, M.; Suzuki, M. *Bull. Chem. Soc. Jpn.* **2015**, *88*, 1093–1099.
- (30) Flanagan, J. C. A.; Kang, E. J.; Strong, N. I.; Waymouth, R. M. *ACS Catal.* **2015**, *5*, 5328–5332.
- (31) Nzahou Ottou, W.; Bourichon, D.; Vignolle, J.; Wirotius, A.-L.; Robert, F.; Landais, Y.; Sotiropoulos, M.-M.; Miqueu, K.; Taton, D. *Chem. - Eur. J.* **2014**, *20*, 3989–3997.
- (32) Matsuoka, S.-I.; Namera, S.; Washio, A.; Takagi, K.; Suzuki, M. *Org. Lett.* **2013**, *15*, 5916–5919.
- (33) Zhang, Y.; Schmitt, M.; Falivene, L.; Caporaso, L.; Cavallo, L.; Chen, E. Y.-X. *J. Am. Chem. Soc.* **2013**, *135*, 17925–17942.
- (34) Naumann, S.; Schmidt, F. G.; Schowner, R.; Frey, W.; Buchmeiser, M. R. *Polym. Chem.* **2013**, *4*, 2731–2740.
- (35) Ottou, W. N.; Bourichon, D.; Vignolle, J.; Wirotius, A.-L.; Robert, F.; Landais, Y.; Sotiropoulos, J.-M.; Miqueu, K.; Taton, D. *Chem. - Eur. J.* **2015**, *21*, 9447–9453.
- (36) Chang, H.-T.; Fréchet, J. M. J. *J. Am. Chem. Soc.* **1999**, *121*, 2313–2314.
- (37) (a) Breslow, D. S.; Hulse, G. E.; Matlack, A. S. *J. Am. Chem. Soc.* **1957**, *79*, 3760–3763. (b) Matlack, A. S. *US Patent*, 2,672,480, 1954.
- (38) Bush, L. W.; Breslow, D. S. *Macromolecules* **1968**, *1*, 189–190.
- (39) Saegusa, T.; Kobayashi, S.; Kimura, Y. *Macromolecules* **1974**, *7*, 256–258.
- (40) Saegusa, T.; Kobayashi, S.; Kimura, Y. *Macromolecules* **1975**, *8*, 950–952.
- (41) (a) Kadokawa, J.-I.; Ikuma, K.; Tagaya, H. *J. Macromol. Sci., Part A: Pure Appl. Chem.* **2002**, *A39*, 879–888. (b) Kadokawa, J.-I.; Kaneko,

Y.; Yamada, S.; Ikuma, K.; Tagaya, H.; Chiba, K. *Macromol. Rapid Commun.* **2000**, *21*, 362–368.

(42) (a) Gibas, M.; Korytkowska-Walach, A. *Polym. Bull.* **2003**, *51*, 17–22. (b) Gibas, M.; Korytkowska-Walach, A. *Polymer* **2003**, *44*, 3811–3816.

(43) Jia, Z.; Yan, D. *J. Polym. Sci., Part A: Polym. Chem.* **2005**, *43*, 3502–3509.

(44) Lin, Y.; Dong, Z.-M.; Liu, X.-H.; Li, Y.-S. *J. Polym. Sci., Part A: Polym. Chem.* **2007**, *45*, 4309–4321.

(45) Matsuoka, S.-I.; Namera, S.; Suzuki, M. *Polym. Chem.* **2015**, *6*, 294–301.

(46) Emrick, T.; Chang, H.-T.; Fréchet, J. M. J.; Woods, J.; Baccei, L. *Polym. Bull.* **2000**, *45*, 1–7.

(47) Gong, C.; Fréchet, J. M. J. *Macromolecules* **2000**, *33*, 4997–4999.

(48) Hecht, S.; Emrick, T.; Fréchet, J. M. J. *Chem. Commun.* **2000**, 313–314.

(49) Gadwal, I.; Binder, S.; Stuparu, M. C.; Khan, A. *Macromolecules* **2014**, *47*, 5070–5080.

(50) Rozenberg, B. A. *Polym. Sci., Ser. C* **2007**, *49*, 355–385.

(51) Hong, M.; Chen, E. Y.-X. *Angew. Chem., Int. Ed.* **2014**, *53*, 11900–11906.

(52) (a) Johnson, K. G.; Yang, L. S. Preparation, Properties and Applications of Unsaturated Polyester. In *Modern Polyesters*; Scheirs, J., Long, T. E., Eds.; Wiley: Chichester, UK, 2003; pp 699–713.

(b) Boenig, H. V. *Unsaturated Polyesters: Structure and Properties*; Elsevier: Amsterdam, The Netherlands, 1964.

(53) See the [Supporting Information](#) for experimental and characterization details.

(54) (a) Feng, S.; Schmitt, M.; Chen, E. Y.-X. *Macromol. Chem. Phys.* **2015**, *216*, 1421–1430. (b) He, J.; Zhang, Y.; Chen, E. Y.-X. *J. Polym. Sci., Part A: Polym. Chem.* **2013**, *51*, 2793–2803. (c) Oishi, S. S.; Rezende, M. C.; Origo, F. D.; Dimiã, A. J.; Botelho, E. C. *J. Appl. Polym. Sci.* **2013**, *128*, 1680–1686.

(55) Based on a mechanistic hypothesis reported by Matsuoka et al., we explored also another stepwise intermolecular pathway converting 3' to 4, involving first a H-transfer from the C $\alpha$  to the C $\gamma'$  of 3', followed by a transfer from the C $\beta$  to the C $\alpha$ ; see Figure 1 of Matsuoka's paper.<sup>26a</sup> Comparing the energetics involved in the mechanism proposed by Matusoka (see the [SI](#)) with that reported in Scheme 4, the direct H-transfer from C $\beta$  to C $\gamma'$  via transition state 3'-4 is favored.